NUCLEAR DATA AND MEASUREMENTS SERIES

ANL/NDM-101

Cobalt, Fast Neutrons and Physical Models

by

A.B. Smith, P.T. Guenther, J.F. Whalen, and R.D. Lawson

July 1987

ARGONNE NATIONAL LABORATORY,
ARGONNE, ILLINOIS 60439, U.S.A.

NUCLEAR DATA AND MEASUREMENTS SERIES

ANL/NDM-101

COBALT, FAST NEUTRONS AND PHYSICAL MODELS

by

A. B. Smith, P. T. Guenther, J. F. Whalen and R. D. Lawson

July 1987

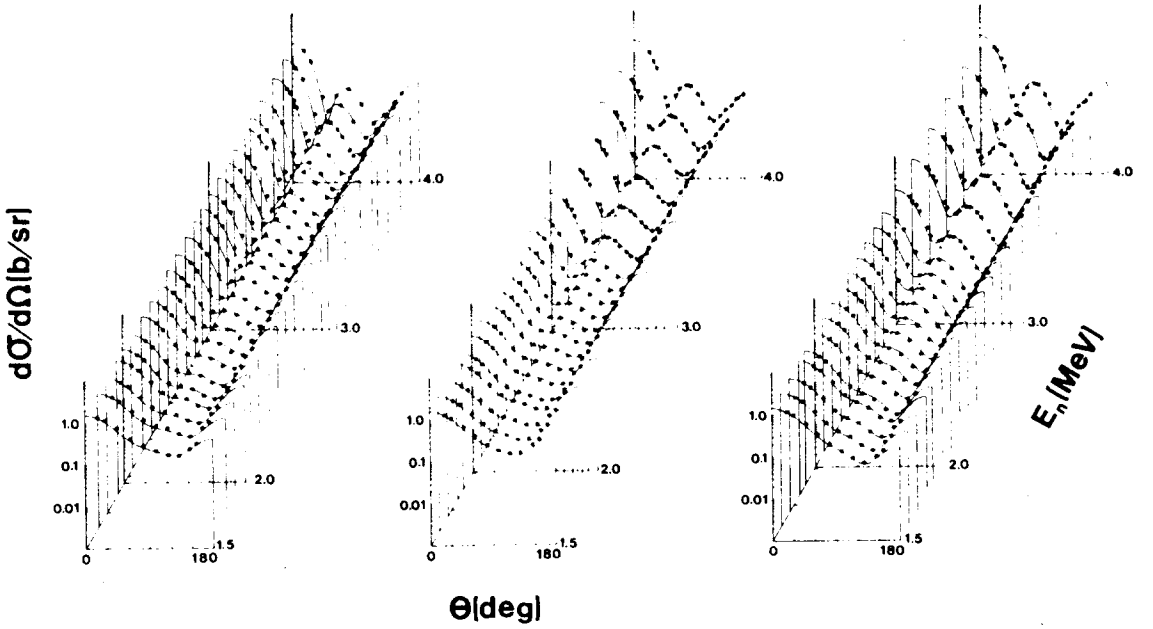

ARGONNE NATIONAL LABORATORY, ARGONNE, ILLINOIS

Operated by THE UNIVERSITY OF CHICAGO

for the U. S. DEPARTMENT OF ENERGY

under Contract W-31-109-Eng-38

ANL/NDM-101

COBALT, FAST NEUTRONS AND PHYSICAL MODELS*

by

A. B. Smith, P. T. Guenther, J. F. Whalen and R. D. Lawson

July 1987

Keywords

Measured σ_t, $d\sigma/d\Omega(E,\theta)$ and $d\sigma/d\Omega(E;E',\theta)$ for neutrons 1-10 MeV. Optical and coupled-channels model interpretations.

* This work supported by the U. S. Department of Energy, Basic Energy Science Programs, under contract W-31-109-ENG-38.

Applied Physics Division
Argonne National Laboratory
9700 South Cass Avenue
Argonne, Illinois
U. S. A.

NUCLEAR DATA AND MEASUREMENTS SERIES

The Nuclear Data and Measurements Series presents results of studies in the field of microscopic nuclear data. The primary objective is the dissemination of information in the comprehensive form required for nuclear technology applications. This Series is devoted to: a) measured microscopic nuclear parameters, b) experimental techniques and facilities employed in measurements, c) the analysis, correlation and interpretation of nuclear data, and d) the evaluation of nuclear data. Contributions to this Series are reviewed to assure technical competence and, unless otherwise stated, the contents can be formally referenced. This Series does not supplant formal journal publication but it does provide the more extensive information required for technological applications (e.g., tabulated numerical data) in a timely manner.

Copies on microfiche can be obtained by contacting:

National Technical Information Service
U.S. Department of Commerce
5285 Port Royal Road
Springfield, Virginia 22161
U.S.A.

INFORMATION ABOUT OTHER ISSUES IN THE ANL/NDM SERIES

A list of titles and authors for reports ANL/NDM-1 through ANL/NDM-50 can be obtained by referring to any report of this Series numbered ANL/NDM-51 through ANL/NDM-76. Requests for a complete list of titles or for copies of previous reports should be directed to:

Section Secretary
Applied Nuclear Physics Section
Applied Physics Division
Building 316
Argonne National Laboratory
9700 South Cass Avenue
Argonne, Illinois 60439
U.S.A.

ANL/NDM-51 A. Smith, P. Guenther, D. Smith and J. Whalen, *Measured and Evaluated Cross Sections of Elemental Bismuth*, April 1980.

ANL/NDM-52 P. Guenther, A. Smith and J. Whalen, *Neutron Total and Scattering Cross Sections of ^{6}Li in the Few-MeV Region*, February 1980.

ANL/NDM-53 James W. Meadows and Donald L. Smith, *Neutron-source Investigations in Support of the Cross-section Program at the Argonne Fast-neutron Generator*, May 1980.

ANL/NDM-54 A.B. Smith, P.T. Guenther and J.F. Whalen, *The Nonelastic-scattering Cross Sections of Elemental Nickel*, June 1980.

ANL/NDM-55 M.M. Bretscher and D.L. Smith, *Thermal-neutron Calibration of a Tritium Extraction Facility using the $^{6}Li(n,t)^{4}He/Au(n,\gamma)^{198}Au$ Cross-section Ratio for Standardization*, August 1980.

ANL/NDM-56 P.T. Guenther, A.B. Smith and J.F. Whalen, *Fast-neutron Interaction with ^{182}W, ^{184}W and ^{186}W*, December 1980.

ANL/NDM-57 Peter T. Guenther, Alan B. Smith and James F. Whalen, *The Total, Elastic- and Inelastic-scattering Fast-neutron Cross Sections of Natural Chromium*, January 1981.

ANL/NDM-58 W.P. Poenitz, *Review of Measurement Techniques for the Neutron-capture Process*, August 1981.

ANL/NDM-59 Wolfgang P. Poenitz, *Review of the Importance of the Neutron-capture Process in Fission Reactors*, July 1981.

ANL/NDM-60 James W. Meadows and Donald L. Smith, *Gamma-ray Detector Calibration Methods Utilized in the Argonne FNG Group Activation Cross-section Measurement Program*, April 1984.

ANL/NDM-61 Carl Budtz-Joergensen, Peter T. Guenther, Alan B. Smith and James F. Whalen, *Fast-neutron Total and Scattering Cross Sections of ^{58}Ni*, September 1981.

ANL/NDM-62 Donald L. Smith, *Covariance Matrices and Applications to the Field of Nuclear Data*, November 1981.

ANL/NDM-63 Alan B. Smith and Peter T. Guenther, *On Neutron Inelastic-scattering Cross Sections of ^{232}Th, ^{233}U, ^{235}U, ^{238}U, ^{239}U and ^{239}Pu and ^{240}Pu*, January 1982.

ANL/NDM-64 James W. Meadows and Carl Budtz-Joergensen, *The Fission-fragment Angular Distributions and Total Kinetic Energies for $^{235}U(n,f)$ from 0.18 to 8.83 MeV*, January 1982.

ANL/NDM-65 Alan B. Smith and Peter T. Guenther, *Note on the Elastic Scattering of Several-MeV Neutrons from Elemental Calcium*, March 1982.

ANL/NDM-66 Alan B. Smith and Peter T. Guenther, *Fast-neutron Scattering Cross Sections of Elemental Silver*, May 1982.

ANL/NDM-67 Donald L. Smith, *Non-evaluation Applications for Covariance Matrices*, July 1982.

ANL/NDM-68 Alan B. Smith, Peter T. Guenther and James F. Whalen, *Fast-neutron Total and Scattering Cross Sections of ^{103}Rh*, July 1982.

ANL/NDM-69 Alan B. Smith and Peter T. Guenther, *Fast-neutron Scattering Cross Sections of Elemental Zirconium*, December 1982.

ANL/NDM-70 Alan B. Smith, Peter T. Guenther and James F. Whalen, *Fast-neutron Total and Scattering Cross Sections of Niobium*, July 1982.

ANL/NDM-71 Alan B. Smith, Peter T. Guenther and James F. Whalen, *Fast-neutron Total and Scattering Cross Sections of Elemental Palladium*, June 1982.

ANL/NDM-72 Alan B. Smith and Peter T. Guenther, *Fast-neutron Scattering from Elemental Cadmium*, July 1982.

ANL/NDM-73 C. Budtz-Joergensen, Peter T. Guenther and Alan B. Smith, *Fast-neutron Elastic-scattering Cross Sections of Elemental Tin*, July 1982.

ANL/NDM-74 Wolfgang Poenitz, Alan B. Smith and Robert Howerton, *Evaluation of the ^{238}U Neutron Total Cross Section*, December 1982.

ANL/NDM-75 A.B. Smith, P.T. Guenther and J.F. Whalen, *Neutron Total and Scattering Cross Sections of Elemental Antimony*, September 1982.

ANL/NDM-76 Alan B. Smith and Peter T. Guenther, *Scattering of Fast Neutrons from Elemental Molybdenum*, November 1982.

ANL/NDM-77 Donald L. Smith, *A Least-squares Method for Deriving Reaction Differential Cross Section Information from Measurements Performed in Diverse Neutron Fields*, November 1982.

ANL/NDM-78 A.B. Smith, P.T. Guenther and J.F. Whalen, *Fast-neutron Total and Elastic-scattering Cross Sections of Elemental Indium*, November 1982.

ANL/NDM-79 C. Budtz-Joergensen, P. Guenther, A. Smith and J. Whalen, *Few-MeV Neutrons Incident on Yttrium*, June 1983.

ANL/NDM-80 W.P. Poenitz and J.F. Whalen, *Neutron Total Cross Section Measurements in the Energy Region from 47 keV to 20 MeV*, July 1983.

ANL/NDM-81 D.L. Smith and P.T. Guenther, *Covariances for Neutron Cross Sections Calculated Using a Regional Model Based on Elemental-model Fits to Experimental Data*, November 1983.

ANL/NDM-82 D.L. Smith, *Reaction Differential Cross Sections from the Least-squares Unfolding of Ratio Data Measured in Diverse Neutrons Fields*, January 1984.

ANL/NDM-83 J.W. Meadows, *The Fission Cross Sections of Some Thorium, Uranium, Neptunium and Plutonium Isotopes Relative to* ^{235}U, October 1983.

ANL/NDM-84 W.P. Poenitz and J.W. Meadows, ^{235}U *and* ^{239}Pu *Sample-mass Determinations and Intercomparisons*, November 1983.

ANL/NDM-85 D.L. Smith, J.W. Meadows and I. Kanno, *Measurement of the* $^{51}V(n,p)^{51}Ti$ *Reaction Cross Section from Threshold to 9.3 MeV*, June 1984.

ANL/NDM-86 I. Kanno, J.W. Meadows and D.L. Smith, *Energy-differential Cross-section Measurement for the* $^{51}V(n,\alpha)^{48}Sc$ *Reaction*, July 1984.

ANL/NDM-87 D.L. Smith, J.W. Meadows, M.M. Bretscher and S.A. Cox, *Cross-section Measurement for the* $^{7}Li(n,n't)^{4}He$ *Reaction at 14.74 MeV*, September 1984.

ANL/NDM-88 A.B. Smith, D.L. Smith and R.J. Howerton, *An Evaluated Nuclear Data File for Niobium*, March 1985.

ANL/NDM-89 Bernard P. Evain, Donald L. Smith and Paul Lucchese, *Compilation and Evaluation of 14-MeV Neutron-activation Cross Sections for Nuclear Technology Applications: Set I*, April 1985.

ANL/NDM-90 D.L. Smith, J.W. Meadows and P.T. Guenther, *Fast-neutron-spectrum Measurements for the Thick-target* $^{9}Be(d,n)^{10}b$ *Reaction at* E_d = 7 *MeV*, April 1985.

ANL/NDM-91 A.B. Smith, P.T. Guenther and R.D. Lawson, *On the Energy Dependence of the Optical Model of Neutron Scattering from Niobium*, May 1985.

ANL/NDM-92 Donald L. Smith, *Nuclear Data Uncertainties (Vol.-I): Basic Concepts of Probability*, April 1986.

ANL/NDM-93 D.L. Smith, J.W. Meadows and M.M. Bretscher, *Integral Cross-section Measurements for* $^{7}Li(n,n't)^{4}He$, $^{27}Al(n,p)^{27}Mg$, $^{27}Al(n,\alpha)^{24}Na$, $^{58}Ni(n,p)^{58}Co$ *and* $^{60}Ni(n,p)^{60}Co$ *Relative to* ^{238}U *Neutron Fission in the Thick-target* $^{9}Be(d,n)^{10}B$ *Spectrum at* E_d = 7 *MeV*, October 1985.

ANL/NDM-94 A.B. Smith, D.L. Smith, P. Rousset, R.D. Lawson and R.J. Howerton, *Evaluated Neutronic Data File for Yttrium*, January 1986.

ANL/NDM-95 Donald L. Smith and James W. Meadows, *A Facility for High-intensity Neutron Irradiations Using Thick-target Sources at the Argonne Fast-neutron Generator*, May 1986.

ANL/NDM-96 M. Sugimoto, A.B. Smith and P.T. Guenther, *Ratio of the Prompt-Fission-Neutron Spectrum of Plutonium 239 to that of Uranium 235*, September 1986.

ANL/NDM-97 J.W. Meadows, *The Fission Cross Sections of* ^{230}Th, ^{232}Th, ^{233}U, ^{234}U, ^{236}U, ^{238}U, ^{237}Np, ^{239}Pu *and* ^{242}Pu *Relative* ^{235}U *at 14.74 MeV Neutron Energy*, December 1986.

ANL/NDM-98 J.W. Meadows, *The Fission Cross Section Ratios And Error Analysis For Ten Thorium, Uranium, Neptunium and Plutonium Isotopes at 14.74 MeV Neutron Energy*, March 1987.

ANL/NDM-99 D.L. Smith, *Some Comments on the Effects of Long-Range Correlations in Covariance Matrices for Nuclear Data*, March 1987.

ANL/NDM-100 A. B. Smith, P. T. Guenther and R. D. Lawson, *The Energy Dependence of the Optical-Model Potential for Fast-Neutron Scattering from Bismuth*, May 1987.

TABLE OF CONTENTS

COBALT, FAST NEUTRONS AND PHYSICAL MODELS*

by

A. B. Smith, P. T. Guenther, J. F. Whalen and R. D. Lawson
Argonne National Laboratory
Argonne, Illinois, USA

ABSTRACT

Energy-averaged neutron total cross sections of cobalt were measured from ≈ 0.5 to 12.0 MeV. Differential elastic- and inelastic-scattering cross sections were measured from ≈ 1.5 to 10.0 MeV over the scattering-angle range ≈ 18^{o} to 160^{o}, with sufficient detail to define the energy-averaged behavior. Inelastic neutron groups were observed corresponding to "levels" at: 1115 ± 29, 1212 ± 24, 1307 ± 24, 1503 ± 33, 1778 ± 40, 2112 ± 40, 2224 ± 35, 2423 ± 39, 2593 ± 41 and 2810 keV. The experimental results were interpreted in terms of the spherical optical-statistical and coupled-channels models. An unusually successful description of observables was achieved over a wide energy range (<-15.0 to > 20.0 MeV) with a spherical model having energy-dependent strengths and geometries. The energy dependencies are large below ≈ 7.0 MeV (i.e., ≈ 19.0 MeV above the Fermi energy), but become smaller and similar to those reported for "global" potentials at higher energies. The imaginary strength is large and decreases with energy. These imaginary-potential characteristics are attributed to neutron shell closure and collective-vibrational processes. The latter are consistent with a weak-coupling model wherein the $f_{7/2}$ proton hole is coupled to the yrast 2^{+} state in ^{60}Ni, and with the observed inelastic scattering which clearly displays a non-statistical component. The weak-coupling model also offers an explanation of the unusual negative energy slope and relatively small radius of the imaginary potential. The spherical optical model derived from the neutron-scattering results was extrapolated to bound energies using the dispersion relationship and the method of moments. The resulting real-potential strength and radius peak at ≈ -10.0 MeV, while concurrently the real diffuseness is at a minimum. The extrapolated potential is ≈ 8% larger than that implied by reported particle-state energies, and ≈ 13% smaller than indicated by hole-state energies.

* This work supported by the U. S. Department of Energy, Basic Energy Science, under Contract W-31-109-Eng-38.

I. INTRODUCTION

For many years the interaction of few-MeV neutrons with nuclei of mass A = 50 to 60 has been somewhat of an enigma. Spherical-optical and/or coupled-channels models, deduced from higher-energy neutron and charged-particle observations, often do not reasonably extrapolate to lower energies. The higher-energy models characteristically over predict the neutron total cross sections at a few MeV.[1,2] Moreover, reasonable descriptions of the neutron total and scattering cross sections over the first few MeV frequently imply sharp energy dependencies of the potential that are inconsistent with potentials based upon higher-energy observations.[3,4] Optical potentials based upon low-energy neutron phenomena tend to be characterized by a small real-potential strength and large real radius, relative to those of higher-energy potentials, and often the real radius exceeds that of the imaginary potential by significant amounts.[5,6] The two types of potentials are qualitatively different, and an abrupt transition from one to the other is often observed at several MeV when attempting to interpret a data base extending from low neutron energies to 10.0 MeV or more with fixed geometries. Linear energy extrapolation of the higher-energy potentials to bound energies is also unsatifying as the strengths implied by known bound particle- and hole-states observed in stripping and pickup reactions are not well described.[7]

Some of the above shortcomings have been attributed to fluctuations, in the context of both physical interpretations and experimental observations. The s-wave strength function is large in the A = 50 to 60 region, and fluctuation corrections to statistical compound-nucleus calculations can be of considerable size.[8] Over the few-MeV region compound-nucleus contributions to the interactions are generally large and their reliable calculation requires knowledge of excited states: discrete states at low energies and then statistical level properties at higher energies. The discrete-level properties are not always well known, and the statistical properties are particularly uncertain at low energies (where level densities are relatively small), and they may fluctuate about the average by considerable amounts. Fluctuations no less trouble experimental observations. Measured energy-averaged low-energy neutron total cross sections, comparable with optical-model (OM) predictions, are often distorted toward too low values due to self-shielding effects.[9] The distortions can be large unless considerable care is taken in

the measurements and/or their correction. Fluctuations are also an obstacle in the measurement of neutron energy-averaged partial cross sections. The latter must be made in energy detail and then averaged over energy intervals large compared to those of the fluctuations of the underlying structure. In the A = 50 to 60 region, at approximately 1.0 to 3.0 MeV, the energy interval required to obtain a reasonable average very often includes the opening of several prominent exit channels that qualitatively change the character of the interpretation within the averaging interval. This dichotomy between channel competition and averaging interval makes quantitative interpretation difficult.

Nuclei in the A = 50 to 60 region display some collective properties. The energies, spins and parities of the first few levels are often characteristic of those predicted for vibrational nuclei, though the quadrupole moments are not zero and there are, in some cases, additional levels that are not consistent with such a concept. In addition, photo-nuclear studies suggest that some of these nuclei have collective-rotational properties.[10] Collective motions can lead to complex and little-understood coupling schemes which are a concern in quantitative modeling. In principle, the coupling should be derivable from basic nuclear-structure concepts, but this approach is difficult and not widely exploited. Failure to properly consider collective effects may be the source of some of the discrepancies between observation and calculation, noted above.

In recent publications, Mahaux and Sartor[11,12,13] have used the dispersion relationship[14], relating the real and imaginary OM potentials, together with the moments of these interactions to predict the energy dependence of the real potential in the bound-state regime. Applied to the A ≈ 89 and 208 regions, these concepts indicate a maximum of this potential strength at bound energies and also a strong energy dependence of the geometric parameters at low-positive and bound energies. In the neighborhood of the Fermi energy the resulting potential is considerably different from that obtained by extrapolating conventional "global" potentials[15], or from the general energy dependence resulting from a Hartree-Fock calculation. This behavior is known as the Fermi Surface Anomoly.[16] In particular, a much more rapid decrease of the real-potential strength is predicted at low positive energies than at higher energies. This is consistent with the dichotomy between the energy dependencies of potentials based upon low- and high-energy neutron

data.[3,4,17,18] In addition, the energy dependence of the potential brings about qualitative agreement with the potential strengths implied by the observed energies of particle and hole states. The above considerations have given emphasis to the A = 208 region, and, to a lesser extent, to the A = 90 region.[12,13,17] The consequence of applying these concepts in the A ≈ 50 to 60 region has not been examined. It is known from low-energy neutron scattering studies that the imaginary-potential strength is mass dependent[19], and low-energy (p,n) studies suggest that the imaginary strengths are particularly large in the A ≈ 60 region.[20]

The present study of the fast-neutron interaction with cobalt was undertaken to cast light on the above outstanding issues. Cobalt is an attractive monoisotopic element for such an endeavor. It is an odd nucleus with a reasonably-high level density at low energies, thus mitigating problems due to fluctuations. Its low-lying level structure displays some characteristics of a collective vibrator, and the respective excited levels are reasonably accessable to measurement. There is experimental information dealing with bound particle- and hole-states making possible the extension of the interpretations below the neutron binding energy. The properties of some of the low-lying levels are well known making possible quantitative compound-nucleus calculations. The magnitude of the Fermi energy is large ($E_f \approx -12.3$ MeV), therefore providing a quite different situation from that encountered in the previous studies of potential anomalies in the A ≈ 208 region ($E_f \approx 6$ MeV). The region of most interest in the context of the above issues is below 10.0 MeV, and it is uniquely accessible to the neutron probe. Finally, there are applied reasons for seeking a thorough understanding of the interaction of fast neutrons with cobalt.

II. EXPERIMENTAL METHODS

The experimental methods employed in the present neutron total and scattering-cross-section measurements have been extensively used at the Argonne Tandem Dynamitron. They have been described in detail[9,21-24], thus only a brief outline is given here.

The measurement samples were fabricated of chemically pure cobalt metal (^{59}Co). The total-cross-section samples were formed of 2.5-cm diameter by 0.125-cm thick wafers, stacked to obtain the desired neutron transmissions in the axial direction. The scattering sample was a solid cylinder 2 cm in diameter and 2 cm long.

The ^{7}Li(p,n)^{7}Be and D(d,n)^{3}He source reactions were used in the monoenergetic measurements, and the ^{9}Be(d,n)^{10}B and ^{7}Li(d,n)^{8}Be reactions in the white-source measurements. The sources were pulsed at repetition rates varying from 0.25 to 2.0 MHz, with a pulse duration of approximately 1 nsec. The monoenergetic energy scale was determined to ± 10 keV by control of the energy of the incident ion beam, and the white-source energy scale was determined from the measured time-of-flight of the emitted neutrons.

The total cross sections were deduced from measured transmission[25] using the rotating-sample method and fast timing techniques, as described in reference 9. Flight paths varied from 3 to 17 m, depending on the particular measurements. The method is self normalizing and requires no monitoring of the source intensity. Seven samples were concurrently studied. One of these was always a carbon reference sample which served to verify the cross-section and energy scales of the measurement system.

The neutron-scattering measurements were made using the Argonne ten-angle scattering apparatus.[22-24,26] The time spectra of neutrons scattered over flight paths of ≈ 503 cm were concurrently measured at the ten scattering angles. Two additional time channels provided redundant monitoring of the neutron-source intensity. Relative detector efficiencies were

determined using the spectrum of neutrons emitted from a ^{252}Cf spontaneously-fissioning source.[27] Up to energies of 4.0 MeV, the cross sections were determined relative to the concurrently-measured neutron total cross section of carbon, as described in reference 28. This method is essentially independent of any reference standard. Above 4.0 MeV, the cross sections were determined relative to the well-known H(n,n) scattering standard.[29] The observed scattering cross sections of cobalt and the reference carbon and hydrogen (polyethylene) samples were corrected for mulitple-event, incident-beam-attentuation, and angular-resolution effects using the methods of reference 30. These procedures involved monte-carlo calculations which were pursued through three iterations.

III. EXPERIMENTAL RESULTS

A. Neutron Total Cross Sections

Neutron total cross sections of cobalt were measured from ≈ 500 keV to 12.0 MeV. The objective was energy-averaged cross sections consistent with the concept of the OM and comparable in scope with the results of the neutron-scattering measurements. The detailed definition of neutron resonances was explicitly not sought.

The monoenergetic-source measurements were made over the energy range 0.5 to 4.5 MeV. Incident-neutron energy spreads varied from 50 to 200 keV, and the measurements were made at energy intervals less than the incident-energy spreads. Six cobalt samples were concurrently used in the measurements, providing neutron transmissions ranging from approximately 40% to 85%. Throughout the low-energy region self-shielding effects are a concern and can distort the results by 10% or more.[31] It was assumed that the self-shielding distortion of the cross sections was a linear function of the sample thickness. The observed cross sections, obtained using various sample thicknesses at a given energy, were therefore least-square fitted with a linear function which was then used to extrapolate the observed cross sections to the infinitely-thin-sample limit. This extrapolation may underpredict the limiting values by amounts estimated to be a few percent or less in the present application.[32] The statistical accuracies of the finite-sample cross sections were of that order, except for the thinnest samples where the uncertainties were larger.

The white-source measurements extended from approximately 1.0 to 12.0 MeV. A thick composite $^{9}Be(d,n)$ and $^{7}Li(d,n)$ neutron-producing target was used. As above, the transmissions of six cobalt samples of various thicknesses were concurrently determined. Small corrections (≈ few percent) for self-shielding effects were made to 1.5 MeV, as described above. At higher energies there was no evidence of self-shielding. The overall time resolution of the detection system was approximately 2 nsec, but events were averaged over larger time increments at higher energies where the cross section varies relatively smoothly with energy. The statistical accuracies of the white-source results varied from less than 1% to a few percent, depending upon the energy range.

Throughout both types of total-cross-section measurements care was taken to obtain the best possible energy-averaged magnitudes. Backgrounds were carefully determined and they were inherently small in both measurement methods. Geometries were very good and thus inscattering corrections were negligible. Careful consideration was given to dead-time effects as these can be a concern, particularly in the white-source measurements where the detector response rate was high. Concurrent with all the cobalt measurements, the total cross sections of carbon were routinely determined. Their observed magnitudes, at non-resonance energies, agreed to within ≈ 1% with those given in standard references.[33] Systematic uncertainties due to other identifiable causes (e.g., sample density determinations) were believed to be small (≤ 1%).

Illustrative raw experimental results are given in Fig. 1 where the cross sections obtained with a sample having a transmission of ≈ 40% are shown. Fluctuations are evident, particularly in the better-resolution white-source results. They indicate that the energy scales used in the two types of measurements are consistent. The fluctuations were reduced by averaging the experimental cross sections over 200 keV energy intervals, with the infinitely-thin-sample results indicated by the solid data symbols in Fig. 2. Even in this broad energy average, some fluctuations persist at lower energies. The present results are compared, in Fig. 2, with those previously reported in the literature and as summarized by the evaluated nuclear data file ENDF/B-V.[34] The energy-averaged values of the present work tend to be larger than those given in ENDF/B-V by 5% to 15% over the wide energy range of ≈ 2.5 to 5.0 MeV. This is a very large discrepancy that will impact on other aspects of the evaluated file, and which cannot be reasonably attributed to self-shielding effects. Moreover, the energy dependence of the ENDF/B-V total cross section is not consistent with common physical concepts (e.g., with the general trends predicted by a reasonable OM, as discussed in detail below).

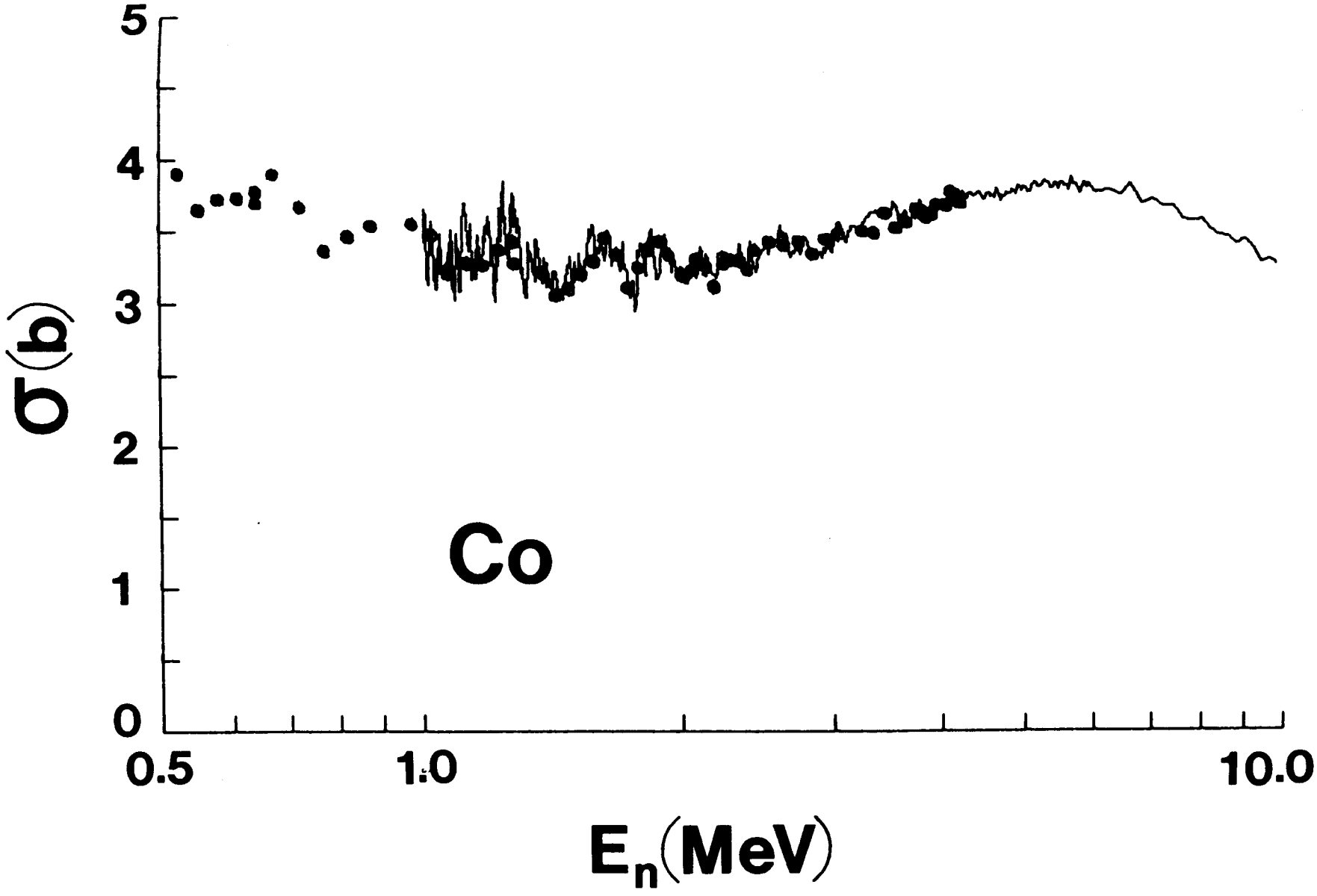

Fig. 1. Observed neutron total cross sections of cobalt obtained using a sample with a transmission of ≈ 40%. The "●" symbols indicate results of monoenergetic measurements and the curve those obtained with the white-source technique.

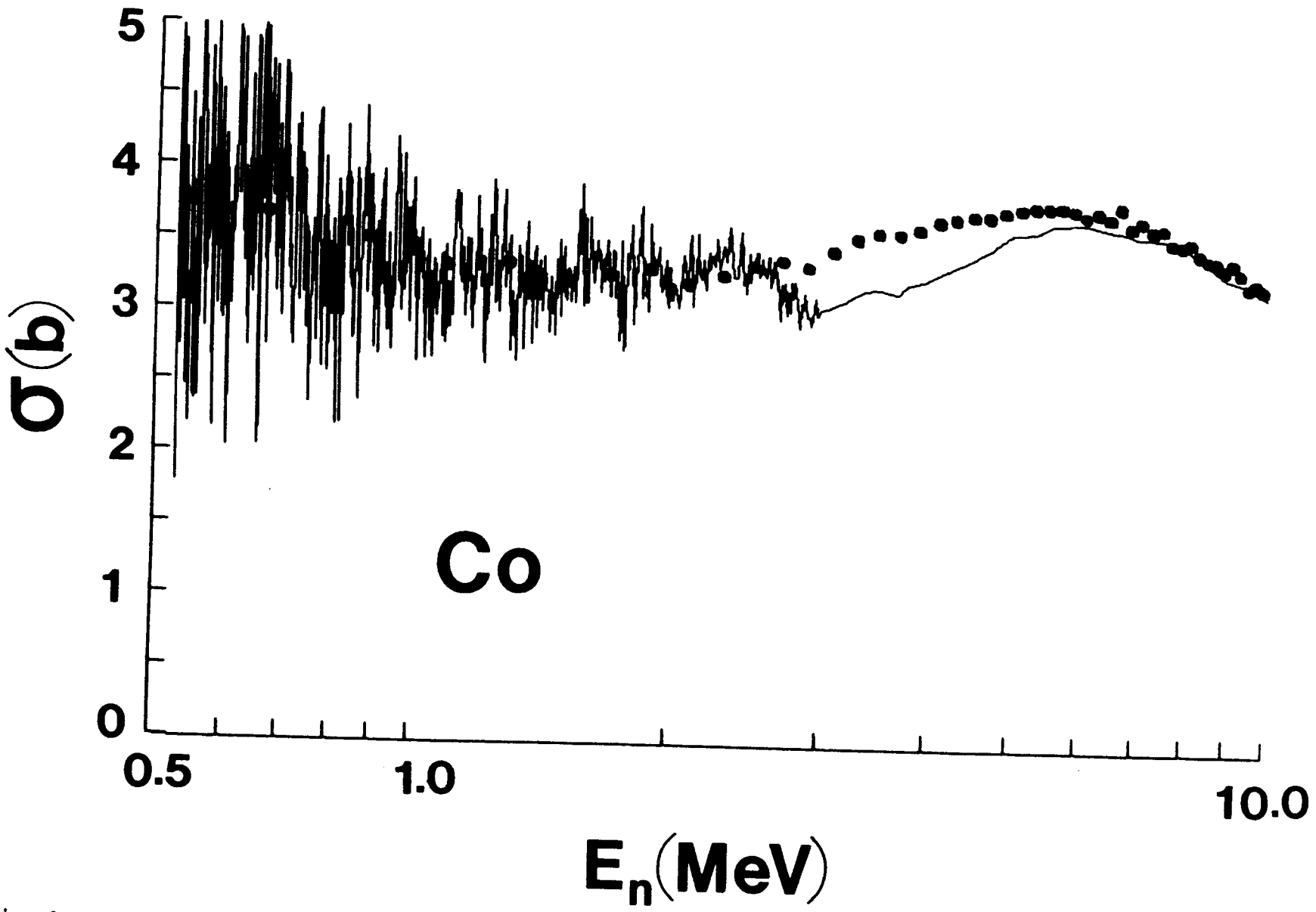

Fig. 2. A comparison of 200-keV averages of the cobalt neutron total cross sections deduced from the present measurements (solid symbols) with the values given by the ENDF/B-V file[34] (curve).

B. Neutron Elastic Scattering

The neutron differential elastic-scattering measurements were made for incident neutron energies of 1.45 to 10.0 MeV.

Up to 4.0 MeV the $^{7}Li(p,n)^{7}Be$ source reaction was used with incident-energy spreads of 50 to 100 keV. The measurements were made at ten scattering angles distributed between $\approx 20^{o}$ and 160^{o} and at incident-neutron energy intervals of $\approx$ 50 keV (i.e., at intervals less than or equivalent to the incident-neutron energy spreads). The statistical uncertainties of the individual cross-section values ranged from less than 1% to several percent. Systematic uncertainties were estimated to be $\leq$ 3%, and uncertainties due to correction procedures were $\leq$ 1%.

Above 4.0 MeV the measurements were made at $\approx$ 500 keV incident-energy intervals, using the $D(d,n)^{3}He$ source reaction, and at 20 to 80 scattering angles distributed between $\approx 18^{o}$ and 160^{o}. The incident-neutron energy spreads decreased from approximately 300 keV at 4.5 MeV to 100 keV at 10.0 MeV. The statistical uncertainties varied from less than 1%, at the very forward scattering angles, to 10% or more at the minima of the higher-energy distributions. Systematic uncertainties were again estimated to be $\approx$ 3%. Uncertainties due to the correction procedures varied from $\approx$ 1% to larger values at the minima of the distributions. Generally, it was assumed that the minimum differential-cross-section uncertainty was 1.5 mb/sr.

For all of the scattering measurements, the relative angular scale was optically determined to $\pm 0.1^{o}$. The reference zero of the angular scale was determined to $\approx \pm 0.3^{o}$ by observing scattering at forward angles both left and right of the center line. This zero uncertainty is a concern in the interpretation of the higher-energy data, as discussed below. Throughout the measurements the incident-neutron energy spreads were intentionally kept broad in order to average cross section fluctuations, while, at the same time, maintaining sufficient scattered-neutron resolution to separate the elastic component from all known inelastic contributions. Even with these relatively broad resolutions, energy-dependent fluctuations were evident in the lower-energy measurements. They were smoothed by averaging the distributions over intervals of 200 keV below 4.0 MeV.

The experimental results are outlined in Fig. 3. The present results reasonably compare with distributions reported in the literature at isolated energies, as illustrated by the examples of Fig. 4, though there are some detailed differences. For example, the agreement with the results of Holmqvist and Wiedling[1] is generally good, except at low energies where fluctuations are a factor. There is good agreement with the results of Kinney and Perey[35], although their values do not extend over the full angle range of the present work. Brandenberger et al.[36] have reported an elastic distribution at ≈ 9.0 MeV. At forward angles their results are in good agreement with those of the present work, but at back angles their values tend to be systematically a few percent larger. The present results are compared with the 1.8 to 4.0 MeV values previously reported from this laboratory[37] in Fig. 5. The present results (A) and those of the previous work (B) are consistent, given the underlying fluctuations, and were combined and averaged to obtain the composite distributions shown in section C of Fig. 5. The present results also reasonably extrapolate to the lower-energy values reported by this group more than twenty years ago[38], as illustrated by the distributions below 1.5 MeV shown in Fig. 3. These various comparisons support the use of the present elastic-scattering data base in the detailed interpretations discussed below.

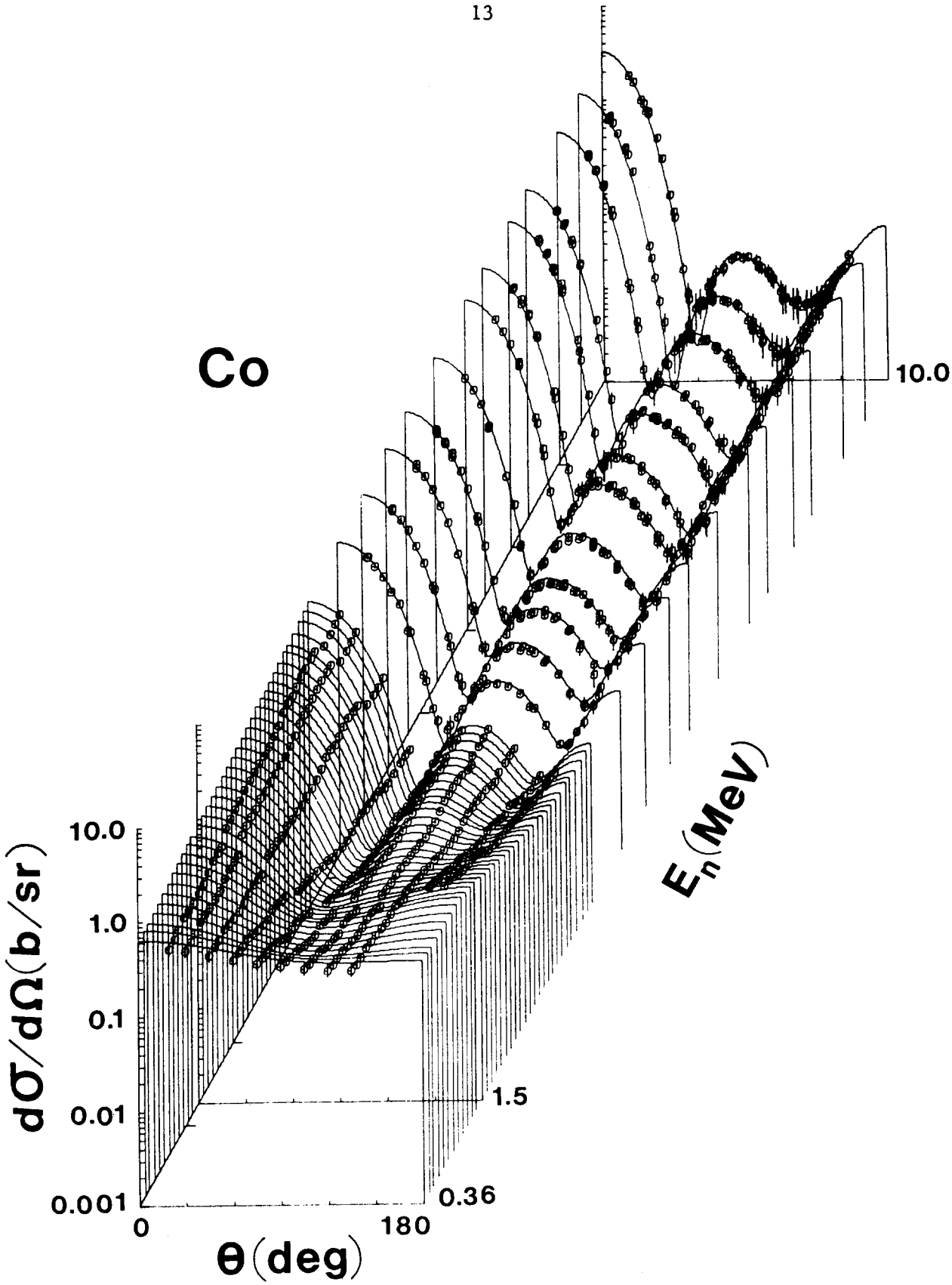

Fig. 3. Differential elastic-scattering cross sections of cobalt. The present results, extending from 1.5 to 10.0 MeV, are indicated by "o" symbols. Results below 1.5 MeV are 200-keV averages of values earlier reported from this laboratory.[38] Curves indicate the results of OM calculations as discussed in the text. All values are given in the laboratory coordinate system.

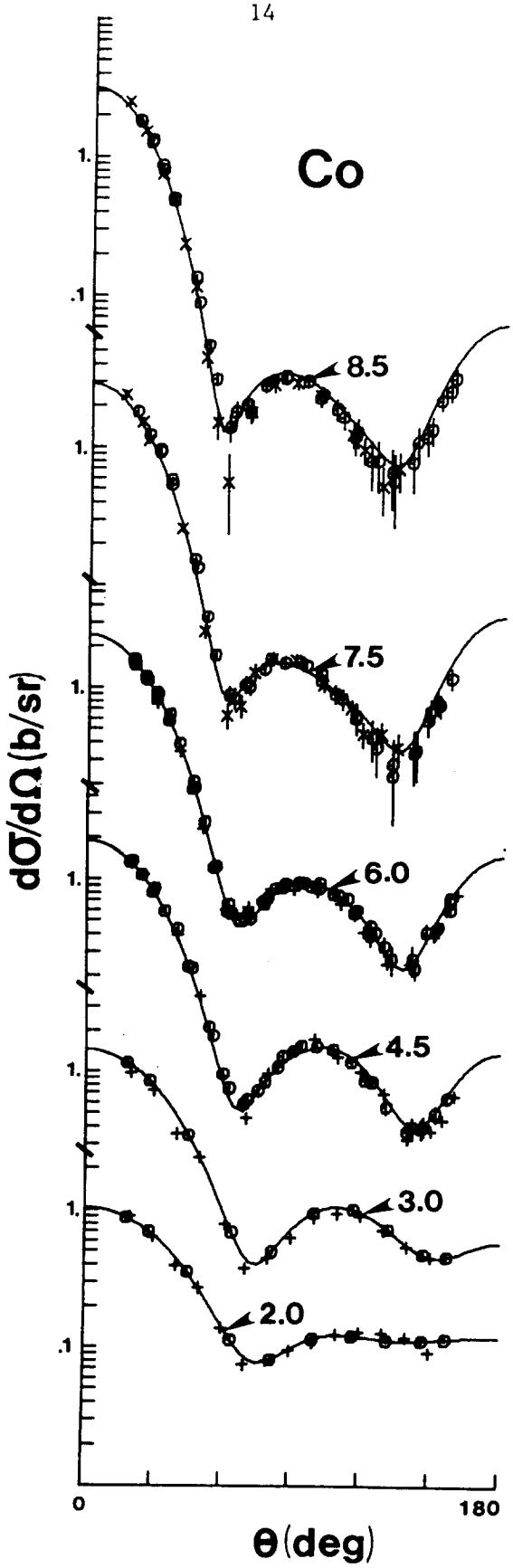

Fig. 4. Illustrative comparisons of measured differential elastic-scattering cross sections of cobalt. The present work is indicated by "o", that of ref. 1 by "+", and that of ref. 35 by "x". Approximate incident-neutron energies are numerically given in MeV, and data are in the laboratory coordinate system.

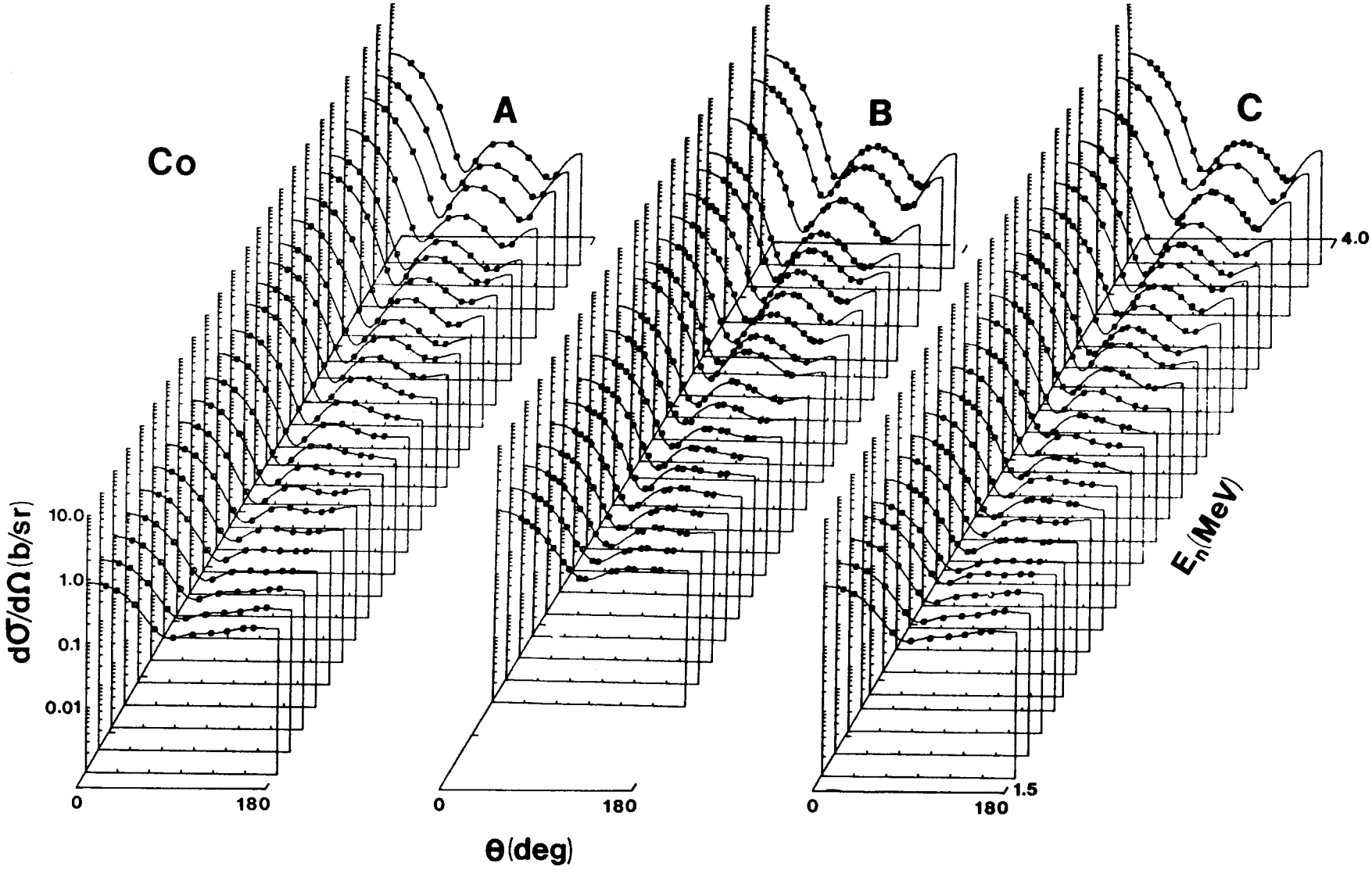

Fig. 5. Differential elastic scattering cross sections of cobalt below 4.0 MeV. The present results (A), those of ref. 37 (B), and a composite average of the two (C) are shown. 200-keV averages of the measured values are indicated by the "o" symbols, curves indicate the results of Legendre-polynomial fits to the data. Fluctuations are evident in all three data sets. Data are given in the laboratory coordinate system.

C. Neutron Inelastic Scattering

Most of the inelastic-scattering measurements were made concurrently with the elastic-scattering determinations (outlined above), using the same relatively-broad incident-neutron energy spreads in order to average fluctuations. These broad energy spreads precluded the resolution of a number of inelastic-neutron groups, and the observed inelastic-scattering cross sections were frequently due to contributions from several components. In order to better define the excited structure, some of the inelastic-scattering measurements were made with much better resolutions (e.g., scattered-neutron resolutions of ≈ 20 keV). A velocity spectrum obtained in one of these better-resolution measurements is shown in Fig. 6. Generally, the measurements were made to within ≈ 600 keV of the respective thresholds and for excitation energies up to ≈ 3.0 MeV. Cross sections for the lower-energy excitations (≤ 1.8 MeV) were determined over the full experimental energy range (i.e., up to 10.0 MeV). Inelastic-neutron groups corresponding to ten "levels" were observed as summarized in Table 1. Some of these undoubtly consisted of two or more components. Table 1 correlates the observations with the levels given in the literature.[39] The cited uncertainties in the experimental excitation energies are the rms deviations of a number of observed values from the respective average, and should not be confused with scattered-neutron resolutions. The general agreement between the observed excitations and those given in the literature is good. The observed differential-inelastic-scattering cross sections were fitted with sixth-order Legendre-polynomial expansions to obtain the angle-integrated inelastic-scattering cross sections shown in Fig. 7. Generally, the scattered-neutron distributions were symmetric about 90^{o}, except for the cross sections of the levels at excitations ≤ 1.8 MeV. The sum of the latter progressively peaked toward forward angles with increasing energy as illustrated in Fig. 8. In addition, the angle-integrated cross sections for the composite of levels with excitations of ≤ 1.8 MeV remained relatively large to at least 10.0 MeV, as illustrated in Fig. 9. The uncertainties associated with the respective angle-integrated cross sections (shown in Figs. 7 and 9) varied from a minimum of 5% to larger values, depending upon the particular experimental conditions. These uncertainties include consideration of statistical, systematic and correction effects, and are believed to be conservative.

There have been a number of previously-reported inelastic-scattering studies of cobalt, as cited in reference 39. Many of these are the result of (n;n',γ) measurements with varying interpretations and frequently discrepant results[40,41,42], as illustrated in Fig. 7. The results of some previously reported (n;n') measurements are compared with the present values in Figs. 7 and 9. The present results are reasonably consistent with those determined from the neutron measurements of reference 37, except for the excitation of the 1190-keV level where the values of reference 37 are somewhat lower. There is reasonable agreement with the lower-energy results of reference 38, good agreement with the neutron measurements of Cranberg and Levin[43] and, at higher energies, with the results of Kinney and Perey.[35]

Table 1. Observed Cobalt Inelastic-Neutron Excitations

N°	E_x(keV) observed[a]	E_x(keV) ref. 39	J-π ref. 39[b]
1	1115 ± 29	1099.9	3/2-
2	1212 ± 24	1190.3	9/2-
3	1307 ± 24	1291.9	3/2-
4.	1503 ± 33	1434.0[c]	1/2-
		1458.9	11/2-
		1481.5	5/2-
5.	1778 ± 40	1744.5	7/2-
6.	2112 ± 40	2061.3[c]	7/2-
		2087.9	5/2-
7.	2224 ± 35	2152.8	7/2-
		2182.4	7/2-
		2205.3	5/2-
8.	2423 ± 39	2395.0	9/2-
9.	2593 ± 41	2478.3	5/2-
		2540.2	(3/2-,5/2-)
		2584.2	(9/2-,11/2-)
10	2810 ± ?	2712.8	1/2+
		2780.7	5/2-
		2825.2	7/2-
		+ others?	

[a] Uncertainties are the rms deviation from the simple mean of a number of measurements.

[b] Spin and parity values used in the calculations. Where there is uncertainty the underlined value was used.

[c] Resolved at selected energies.

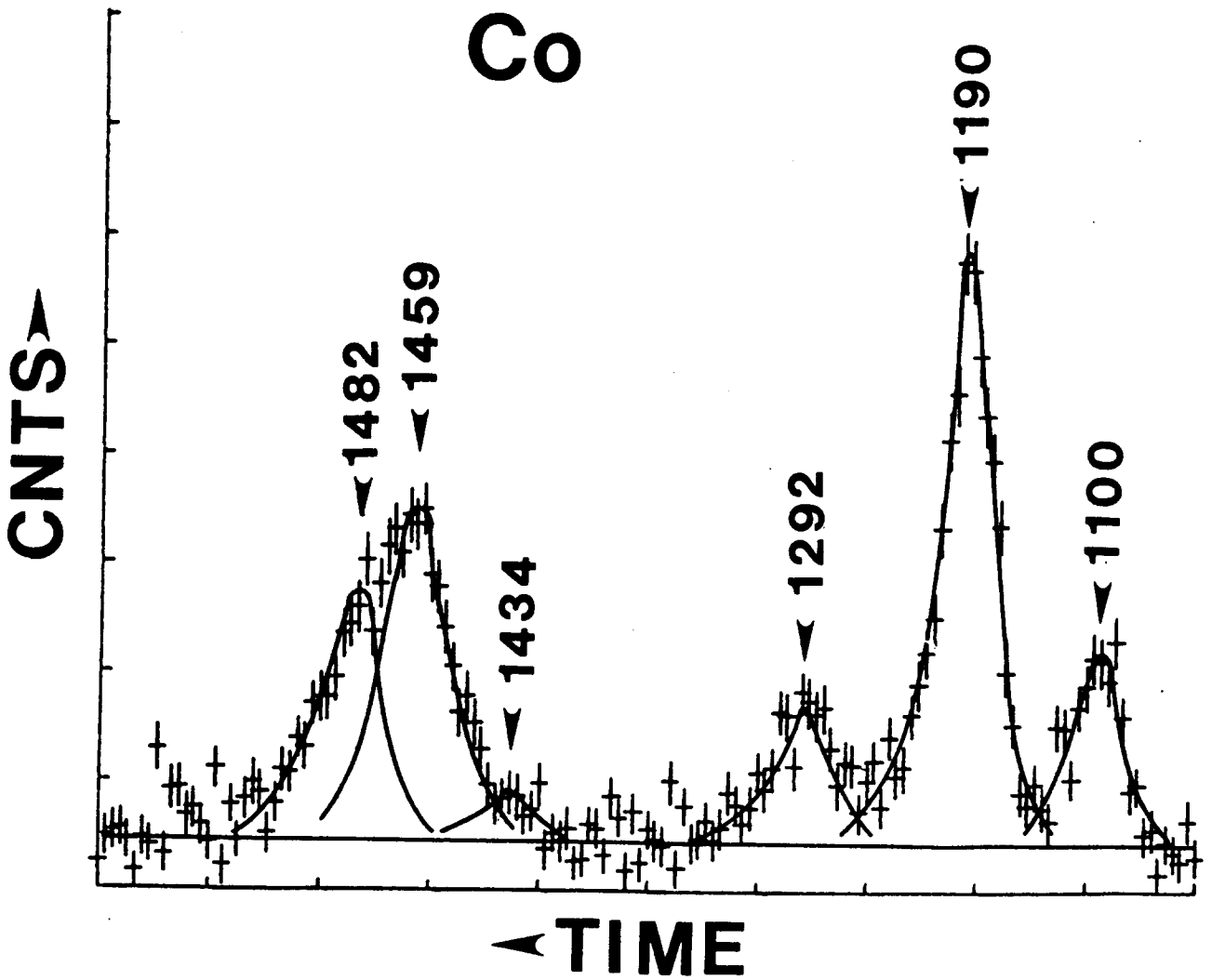

Fig. 6. A good-resolution velocity spectrum obtained at an incident energy of 3.0 MeV. The laboratory scattering angle was $\approx 120^{o}$ and the flight path $\approx$ 503 cm. Level energies are noted numerically in keV. Background is indicated by the horizontal line, time per measurement channel is $\approx$ 1 nsec.

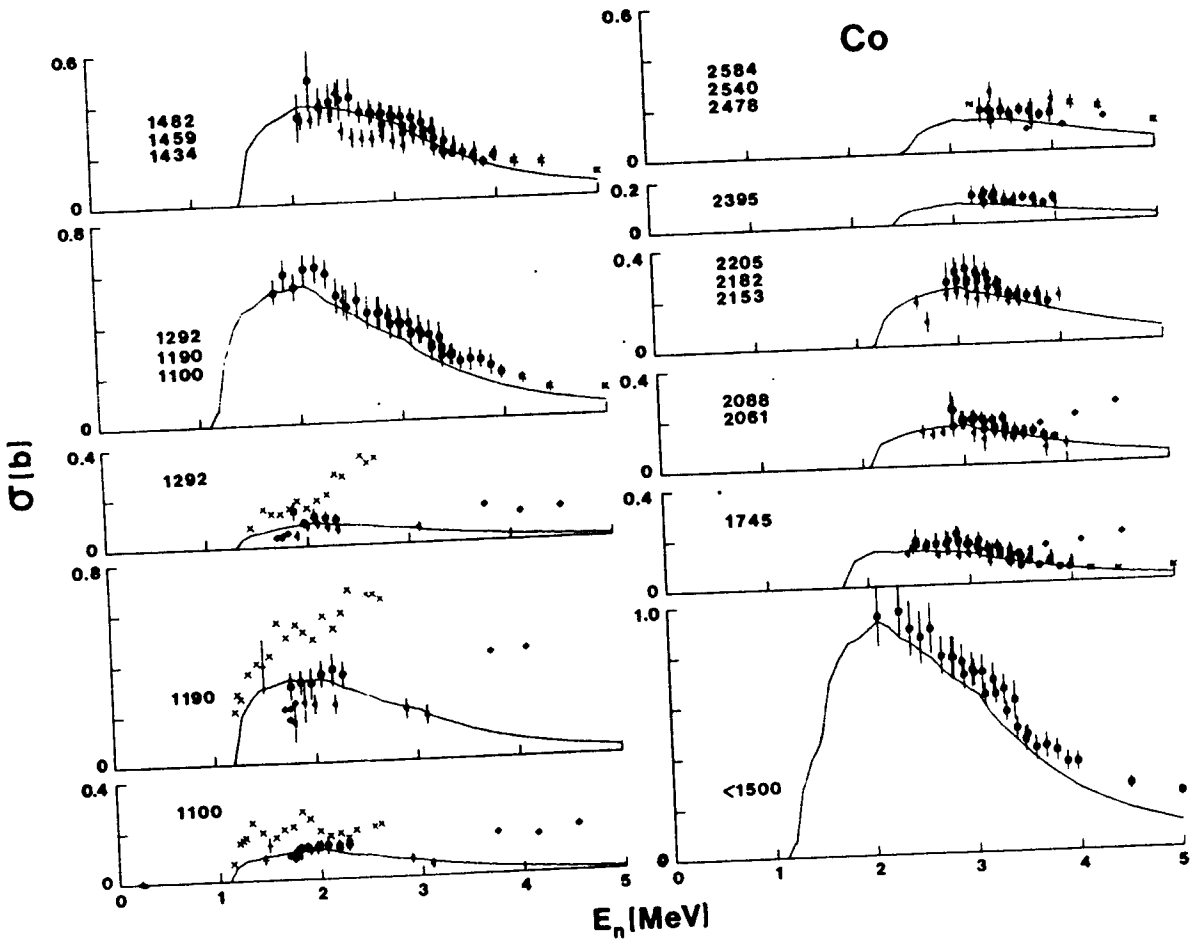

Fig. 7. Angle-integrated inelastic neutron-excitation cross sections of cobalt. Present results are noted by "●". Comparative values from the literature are: ref. 40 = x and ref. 41 = ◇, and ref. 42 = N (results of (n;n',γ) measurements), ref. 37 = ◁, ref. 38 = +, ref. 43 = ←, and ref. 35 = ⋉ (results of direct (n,n') measurements). Curves indicate the results of statistical-model calculations as discussed in the text. Excitation energies (in keV)[39] are numerically given in each section of the figure. The data are in the laboratory coordinate system.

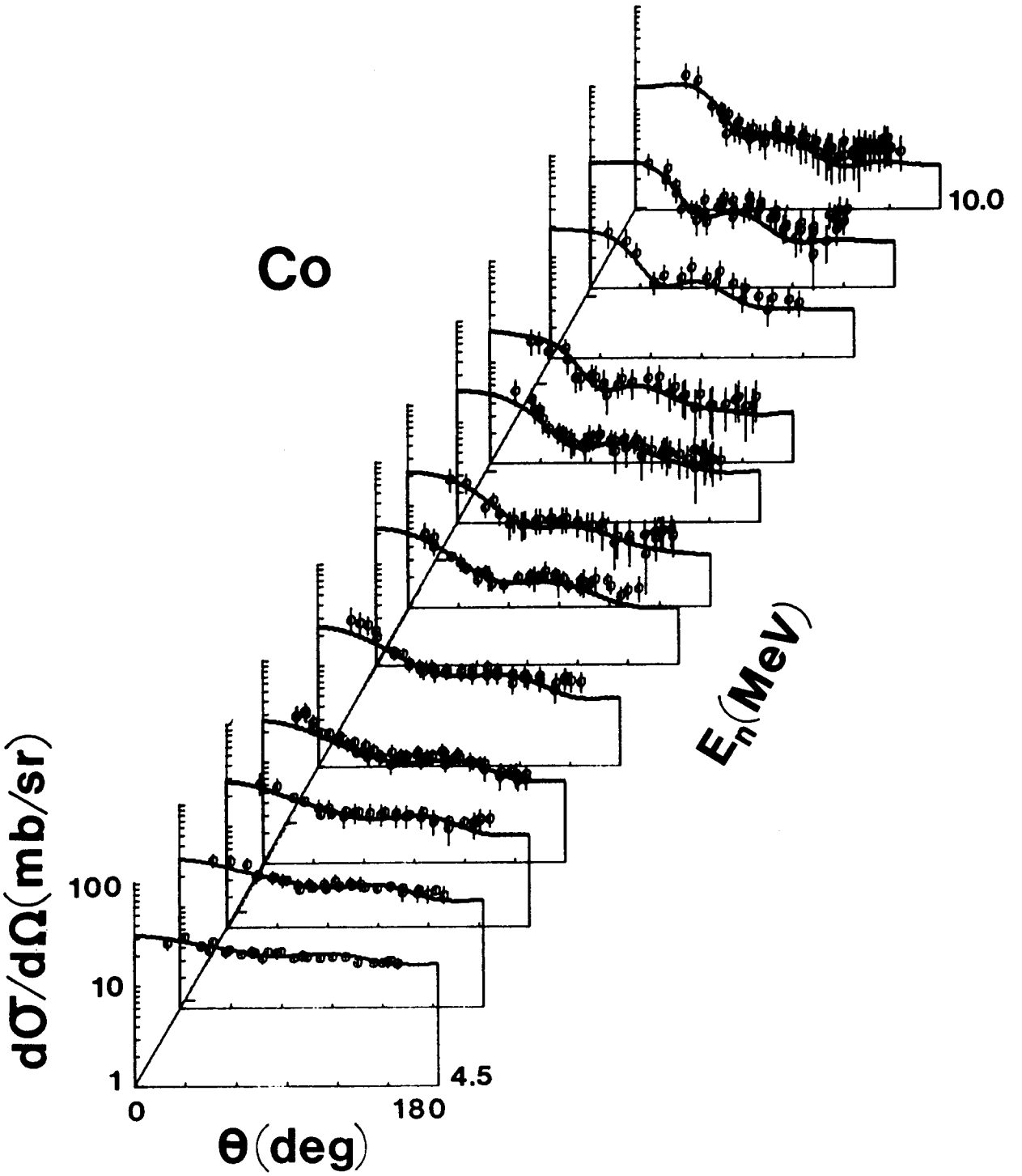

Fig. 8. Differential cross sections for the excitation of the composite of levels in the range E_x = 1.0 to 1.8 MeV. Measured values of the present work are given by "o" symbols, and the results of the calculations described in the text by curves. The data are in the laboratory coordinate system.

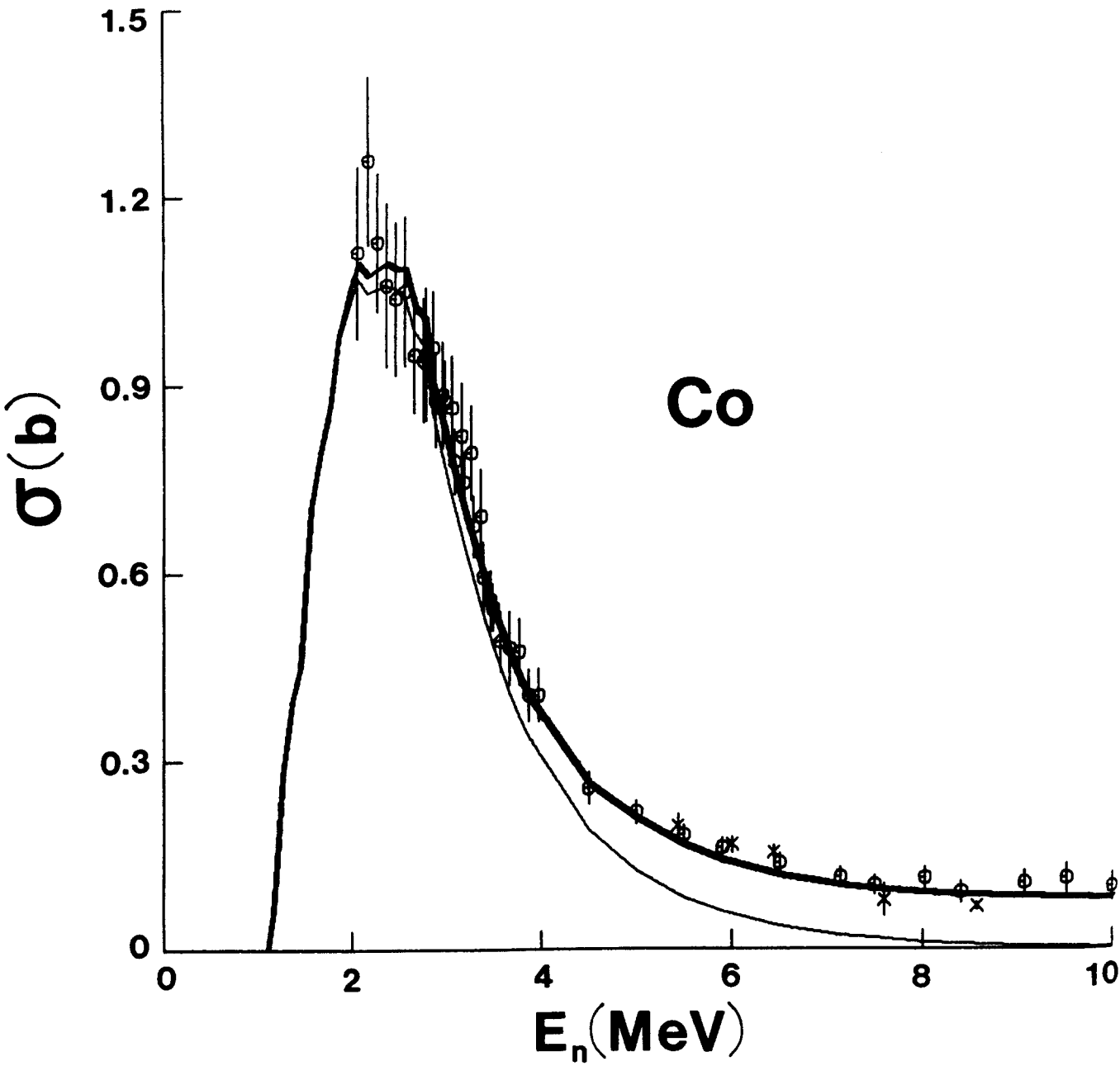

Fig. 9. Angle-integrated cross sections for the excitation of levels in the range E_x = 1.0 to 1.8 MeV. "o" symbols denote the present experimental results and "x" those of reference 35. Results of statistical-model calculations are indicated by the light curve, and those including the vibrational contribution by the heavy curve. The data are in the laboratory coordinate system.

IV. INTERPRETATION

The interpretation was primarily based on the conventional spherical optical-statistical model (OM),[44] explicitly fitting the model parameters to the differential elastic-scattering cross sections. It was assumed that the OM potential had a real Woods-Saxon form, a Woods-Saxon-derivative imaginary part, and a real Thomas spin-orbit term.[44] A possible contribution due to volume absorption was investigated at the higher energies of the present measurements with no identifiable consequences. An imaginary spin-orbit component of the potential was not considered. All of the spherical calculations were carried out with the most recent formulation of the computer code ABAREX.[45]

The OM fitting employed χ^2 minimization procedures (varying up to six parameters, real and imaginary potential strengths, radii, and diffusenesses), minimizing the quantity,

$$\chi^2 = \frac{1}{N} \sum_{i=1}^{N} \left[\frac{\sigma_{exp}(\theta_i) - \sigma_{cal}(\theta_i)}{\delta\sigma_{exp}(\theta_i)} \right]^2, \qquad (1)$$

where $\sigma_{exp}(\theta_i)$ is the measured value at angle θ_i, $\delta\sigma_{exp}(\theta_i)$ its uncertainty, $\sigma_{cal}(\theta_i)$ the corresponding calculated value, and N is the number of data points contained in a given distribution. Up to an energy of $\approx$ 8.0 MeV, compound-nucleus processes make a significant contribution to the elastic scattering. They were calculated using the Hauser-Feshbach formula,[46] with the fluctuation and correlation corrections prescribed by Moldauer.[8] The compound-nucleus calculations included discrete levels up to an excitation energy of 2.6 MeV, using the energies, spins, and parities cited in Table 1. A statistical-level formulation given by

$$\rho(E,J) = \frac{(2J + 1)}{2\sigma^2 T} \exp((E - E_o)/T) \cdot \exp(-(J + 1/2)^2/2\sigma^2), \qquad (2)$$

where J is the angular momentum of the continuum target level and E_o, T and σ are parameters, was used to describe higher-energy excitations. Initially the parameters E_o, T, and σ were taken

from the work of Gilbert and Cameron.[47] However, with their values the inelastic cross sections corresponding to excitations of ≤ 1.8 MeV, shown in Fig. 9, were underestimated by ≈ 15% in the 3.0 to 4.0 MeV incident-energy range, and concurrently the minima of the differential elastic-scattering distributions were systematically smaller than observed. A better agreement between observation and calculation was obtained by increasing T by 40 keV, resulting in the statistical parameters for the subsequent calculations of

$$\begin{aligned} E_o &= -0.4 \text{ MeV} \\ T &= 1.10 \text{ MeV} \\ \sigma &= 3.0. \end{aligned} \qquad (3)$$

Above ≈ 8.4 MeV there was no evidence for a compound-nucleus contribution, so the calculations considered only shape-elastic scattering. Fluctuations are evident in the neutron total and differential-elastic-scattering cross sections to more than 4.0 MeV (e.g., see Figs. 1, 2, 3 and 5), even with the relatively broad incident-energy spreads and the averaging procedures employed in the present measurements. Therefore, primary emphasis in the interpretation was given to the energy range 4.5 to 10.0 MeV, The lower-energy data were concurrently fitted in three energy intervals having widths of ≈ 1.0 MeV. Even so, the parameters resulting from the lower-energy fitting fluctuated by considerable amounts and thus were not used for determining the general behavior of the parameters. At the higher energies the distributions are strongly forward peaked, and thus the fitting was sensitive to small angular uncertainties. These, and the other experimental uncertainties, were carefully assessed as outlined in Sec. III, above. Near zero energy the $\ell = 0$ strength function, S_o, is fairly well known from resonance measurements.[48] This value provides a low-energy reference point in the fitting. The energy-averaged neutron total cross section is reasonably known to at least 20.0 MeV, not only from the present work but also from a comprehensive evaluation of the available experimental information reported elsewhere.[49] Considerations of the total cross section further guided the fitting beyond the primary 4.5 to 10.0 MeV range of the present measurements. In addition, consistency with Wick's Limit [51] was sought.

The present elastic-scattering data were most sensitive to the spin-orbit potential at the higher energies. Therefore, the 9.0 to 10.0 MeV data were used to determine the spin-orbit

potential. Two approaches were used. In the first a mesh of spin-orbit parameters was set up and six-parameter fits to the data were made, concurrently varying real and imaginary strengths, radii and diffusenesses. In the second approach reasonable real and imaginary potentials were assumed and the spin-orbit parameters alone were fitted. The results from both approaches were very similar and the average values were

$$\begin{aligned} V_{so} &= 5.5 \text{ MeV} \\ r_{so} &= 1.005 \text{ fm} \\ a_{so} &= 0.65 \text{ fm}, \end{aligned} \qquad (4)$$

where V_{so} is the strength, r_{so} the radius (herein all radii are expressed in the form $R_i = r_i A^{1/3}$), and a_{so} is the diffuseness. These values were not used to calculate polarization data since no suitable experimental information was found in CINDA[50] or the files of the National Nuclear Data Center.[52] However, the parameters of Eq. (4) are reasonably consistent with those cited in global OM's.[15,53] The values of Eq. (4) were held fixed for the subsequent interpretation.

With the above spin-orbit potential, the fitting started by varying the six parameters, real and imaginary strengths, radii and diffusenesses, using the 4.5 to 10.0 MeV data. The results indicated a relatively constant real diffuseness, a_v, and it was fixed to the average value obtained from the fitting of the distributions. The fitting procedure was then repeated varying the remaining five parameters. Of these, the imaginary diffuseness, a_w, was the most stable and was fixed for the subsequent four parameter fitting. It was evident that a_w was energy dependent, increasing from rather small values at low energies to $\approx$ 7.0 MeV, and then remaining approximately constant at higher energies. This change in behavior at $\approx$ 7.0 MeV was noted in other geometric parameters and will be discussed in Sec. V. The four-parameter fits resulted in reasonable definition of the real radius, r_v. Again, there appeared to be a change in the energy dependence at $\approx$ 7.0 MeV, with a large negative slope below that energy and a small slope at higher energies. The three remaining parameters were then fitted, with results indicating that the imaginary radius, r_w, was $\approx 0.96 \times r_v$. This behavior was not as well determined as that of the other geometric

parameters as the results were not particularly stable below ≈ 5.5 MeV, possibly reflecting underlying fluctuations of the data base. The resulting geometric parameters are summarized by,

$$
\begin{aligned}
r_v &= 1.39 - 0.0168 \cdot E \quad (E \leq 7.5 \text{ MeV}) \quad \text{fm} \\
&= 1.288 - 0.0032 \cdot E \quad (E \geq 7.5 \text{ MeV}) \quad \text{fm}, \\
a_v &= 0.6355 \text{ fm}, \\
r_w &= 0.96 \cdot r_v \quad \text{fm}, \\
a_w &= 0.19 + 0.0386 \cdot E \quad (E \leq 7.5 \text{ MeV}) \quad \text{fm} \\
&= 0.480 \quad (E \geq 7.5 \text{ MeV}) \quad \text{fm},
\end{aligned}
\tag{5}
$$

where E (throughout this work) is the laboratory incident-neutron energy in MeV.

With the above potential geometry, two parameter fits were made, varying the real, V_o, and imaginary, W_o, strengths. The results were expressed as volume-integrals-per-nucleon given by

$$
J_v = \frac{4\pi}{A} \int_o^\infty V(r)\, r^2\, dr
$$

and

$$
J_w = \frac{4\pi}{A} \int_o^\infty W(r)\, r^2\, dr. \tag{6}
$$

They are shown, together with the associated χ^2/point resulting from the individual fits, in Fig. 10. The figure also shows the results obtained from the concurrent fits to the lower-energy data which was averaged over ≈ 1.0 MeV energy intervals. The χ^2/point of the latter are large, in contrast to the 4.5 to 10.0 MeV fits where χ^2/point is of the order of unity. Evidently, both J_v and J_w are not linear functions of energy but rather show a different slope below and above ≈ 7.0 MeV. Combining these results with the requirement that the S_o strength function be well represented and the neutron total cross section be reasonably predicted to at least 20.0 MeV, one concludes that the J_v and J_w results are reasonably described by two linear segments given by

$$J_V = 550.0 - 12.5 \cdot E \quad \text{MeV-fm}^3 \quad (E \leq 7.5)$$

$$= 474.0 - 2.4 \cdot E \quad \text{MeV-fm}^3 \quad (E \geq 7.5)$$

and

$$J_W = 135.0 - 6.4 \cdot E \quad \text{MeV-fm}^3 \quad (E \leq 7.5) \qquad (7)$$

$$= 104.0 - 2.3 \cdot E \quad \text{MeV-fm}^3 \quad (E \geq 7.5).$$

The high-energy behavior is similar to that frequently reported in "global" analyses.[15] The segmented linear representations of Eq. (7) are doubtless an approximation to a smoother energy dependence such as suggested by the dashed curve in Fig. 10, and as further discussed in Sec. V. The uncertainties shown in Fig. 10 for J_V and J_W are respectively 1% and 5%, multiplied by the χ^2/ point at the energy of interest. These uncertainty estimates are reasonably born out by the reproducibility of results obtained at different times.

Eqs. (4), (5), and (7) result in an S_o strength function of 3.97×10^{-4} compared to the value $3.9 (\pm 0.5) \times 10^{-4}$ deduced from resonance data.[48] The same equations give a reasonably good description of the neutron total cross sections from several-hundred keV to 20 MeV, as illustrated in Figs 11 and 12. The former compares the calculated results with a 100 keV average of the total cross section given by a recent experimentally-based evaluation.[49] The agreement is within several percent, except at very low energies, where fluctuations are extremely prominent, and above ≈ 17.0 MeV where the calculations are somewhat lower than the evaluated cross sections. In the latter region there are ambiguities in the experimental data, as illustrated in Fig. 12, where energy averages of the entire experimental data base available at the National Nuclear Data Center[52] are compared with the calculated results. From this figure it is evident that the higher-energy calculated results are consistent with the available experimental values, which in themselves are not in particularly good agreement. It should be noted that the calculations reasonably represent the observed total-cross-section minimum in the 1.0 to 3.0 MeV region, a result which is not obtained when the conventional "global" models primarily based upon high-energy observations are used.[2] This is a reflection of the energy dependence of the potential used in the present calculations. Eqs. (3), (4), (5) and (7) also provide a very good description of the observed neutron

differential elastic-scattering cross sections from less than 1.0 to 10 MeV, as illustrated in Fig. 3. At several-hundred keV the calculated cross-section shape is representative of the measured values but the magnitudes are somewhat larger than that resulting from experiment. This magnitude difference is in a region of large cross-section fluctuations and is also evident in the total-cross-section comparisons of Figs. 11 and 12.

Using Eqs. (3), (4), (5) and (7), together with the J^{π} values of Table 1, the Hauser-Feshbach-Moldauer model[8,46] leads to the calculated excitation functions indicated by the curves of Fig. 7. Up to ≈ 4.0 MeV the calculations are in agreement with the measured values. However, above this energy there is a systematic tendency for the excitation cross sections of the levels below ≈ 1.8 MeV to be underpredicted, and increasingly so with energy. This trend is discussed below. The calculated excitations of these lower-lying levels give a particularly good description of the high-resolution measurements below ≈ 3.0 MeV. This is illustrated by a comparison of Figs. 6 and 13. The latter shows the calculated excitation cross sections at 3.0 MeV, on a suitable time scale and corrected for detector sensitivity so as to make possible direct comparison with the measured spectrum of Fig. 6. The observed relative magnitudes of these closely-spaced scattered-neutron groups are well reproduced by the calculations. The comparisons of measured and calculated results for the excitation of the observed states at ≈ 2593 keV tend to support the $5/2^{-}$ and $9/2^{-}$ J^{π} assignments of Table 1 for the 2540 and 2584 levels, respectively. The alternate values of Table 1 lead to ≈ 10-20% smaller calculated cross sections, tending to be in disagreement with observation. Otherwise, the J^{π} selections of Table 1 appear justified by the comparisons of Fig. 7.

As the energy increases it becomes clear that the simple compound-nucleus concept is deficient. In particular, neutrons resulting from the complex of levels below 1.8 MeV are no longer emitted symmetrically about 90^{o}, as required by a compound-nucleus mechanism (see Fig. 8), but rather the distributions are strongly peaked toward forward angles. The statistical calculations predict very small cross sections for the excitation of this complex of levels above ≈ 5.0 MeV incident energy, and the calculated results are an order of magnitude smaller than the observations at 8.0 to 10.0 MeV (see Fig. 9). This behavior suggests a significant direct-reaction contribution, which can be estimated as follows: Below 2.0 MeV

^{59}Co has seven negative parity states with spins 1/2, (3/2)$^-$, 5/2, 7/2, 9/2 and 11/2. The weak-coupling model, in which an $f_{7/2}$ proton hole is coupled to the first excited 2^+ state in ^{60}Ni, accounts for five of these levels. The remaining two, the $1/2^-$ and one $3/2^-$, are attributed to the excitation of an $f_{7/2}$ proton to either the $p_{1/2}$ or $p_{3/2}$ single-particle state. (In fact, the (^{3}He,d) and (α,t) reactions[54] populate both 3/2 states indicating that there is a single-particle component, as well as weak-coupling part, in each level) Since the yrast 2^+ state in ^{60}Ni is collective, one would expect the majority of the direct-reaction strength in the low-lying ^{59}Co levels to come from the excitation of this state. To estimate this cross section it was assumed that ^{60}Ni is a vibrational nucleus, and a coupled-channels calculation[55] was carried out in which the one-phonon, 1.333 MeV 2^+, and the two-phonon states, the 2^+, 0^+ and 4^+ at 2.159, 2.285 and 2.506 MeV, respectively,[56] were considered. Except for the radius of the imaginary interaction, which was assumed to be 6% larger than given in Eq. (5), the strength and geometry of the deformed potential were taken to be those of Eqs. (4), (5) and (7). (The reason for the change in r_w will be discussed later.) The spin-orbit interaction was taken to be spherical, whereas the deformation of both the real and imaginary interactions was assumed to be described by $\beta_2 = 0.25$. The direct-reaction cross section to the 1.333 MeV state, which would be divided among the weak-coupling $3/2^-$, $5/2^-$, $7/2^-$, $9/2^-$ and $11/2^-$ levels of ^{59}Co, was calculated on the basis of this model. The contribution was then added to the statistical contribution, derived assuming that ^{59}Co is a spherical nucleus, to obtain an estimate of the total inelastic-scattering cross section. The predicted angular distributions of scattered neutrons due to the excitation of the complex of levels below 1.8 MeV, derived in the above manner, agreed fairly well with the experimental values as illustrated in Fig. 8. Furthermore, the predicted total inelastic-scattering cross section for the same complex of levels agrees well with measured values, as shown in Fig. 9. It is, of course, inconsistent to add the deformed contribution to the statistical component calculated using spherical-potential transmission coefficients. However, at 3.0 MeV the statistical contribution changes by only about 30 mb when

the spherical transmission coefficients are replaced with deformed ones. Since the experimental values are uncertain by at least this amount, the inconsistency is unimportant in making comparisons with the data. Thus, over the energy range 1.0 to 10.0 MeV, the scattered-neutron angular distributions and the total inelastic-scattering cross sections for the excitation of the complex of levels in ^{59}Co below 1.8 MeV can be reasonably well described by adding the statistical component, calculated assuming the spherical model, to the direct-reaction cross section for exciting the yrast 2^+ level in ^{60}Ni, assuming the nucleus is a vibrator with $\beta_2 = 0.25$.

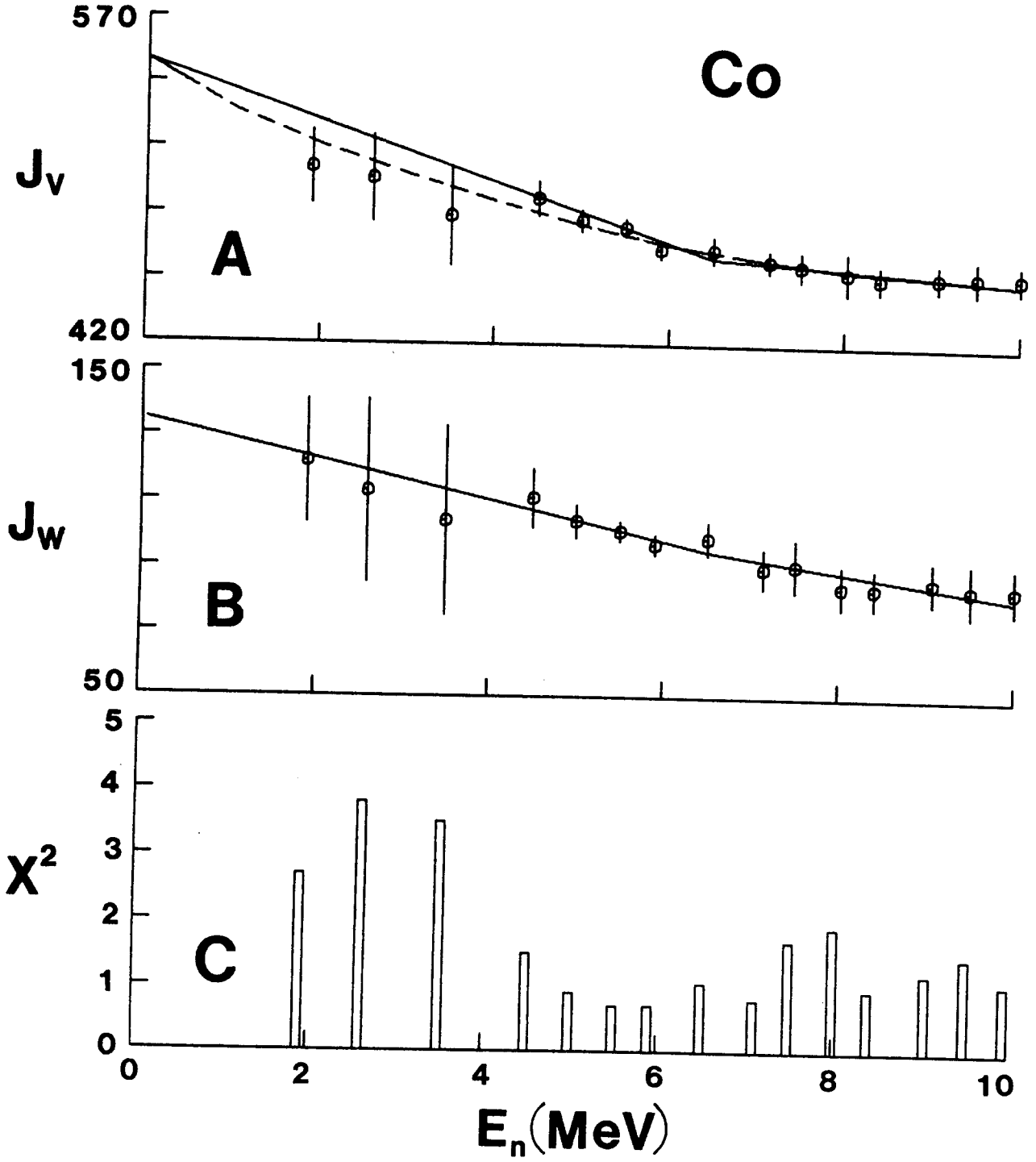

Fig. 10. Sections (A) and (B) show, respectively, the real and imaginary potential strengths, J_v and J_w of Eq. (6) (in MeV-fm^3), as a function of laboratory energy, E_n. Symbols indicate the results of fitting the experimental data and the curves illustrate Eq. (7) of the text. In Section (C), χ^2/point, defined by Eq. (1), is shown at each energy.

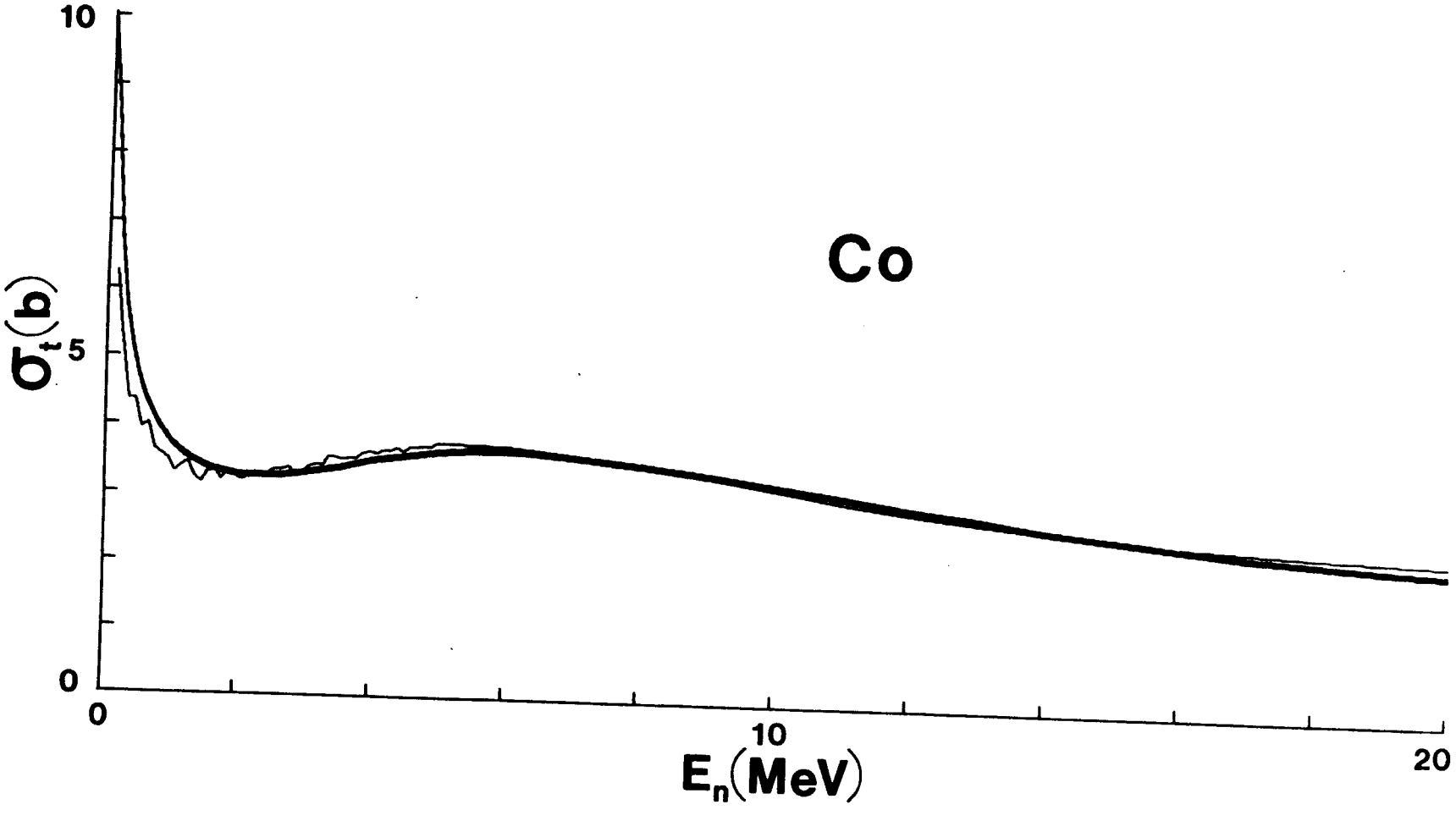

Fig. 11. Comparison of calculated (heavy curve) total cross sections with a 100-keV average of the experimentally-based evaluation of reference 49 (light curve).

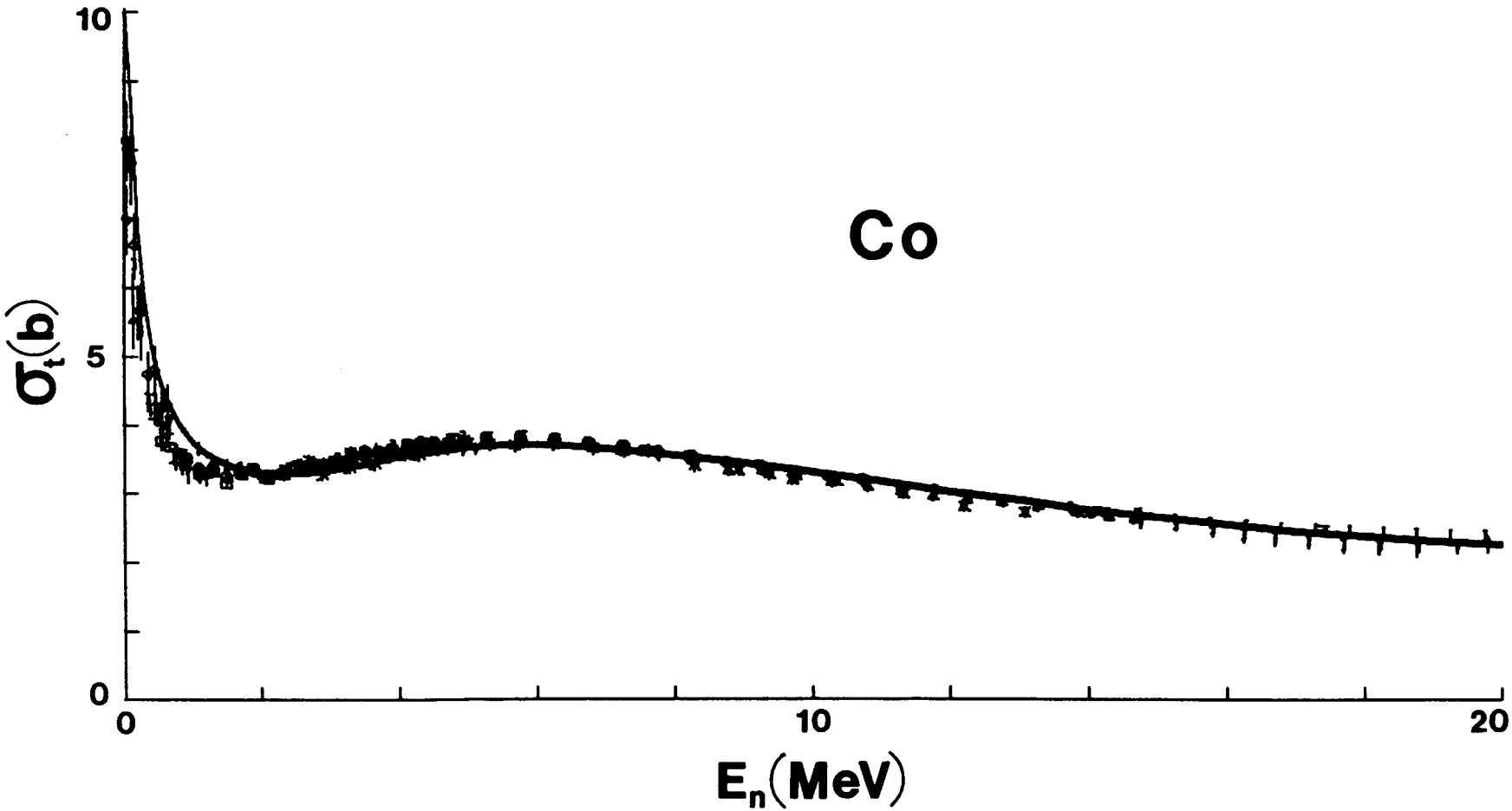

Fig. 12. Comparison of calculated (heavy curve) total cross sections with broad energy averages of all the experimental data available at the National Nuclear Data Center[52] (symbols).

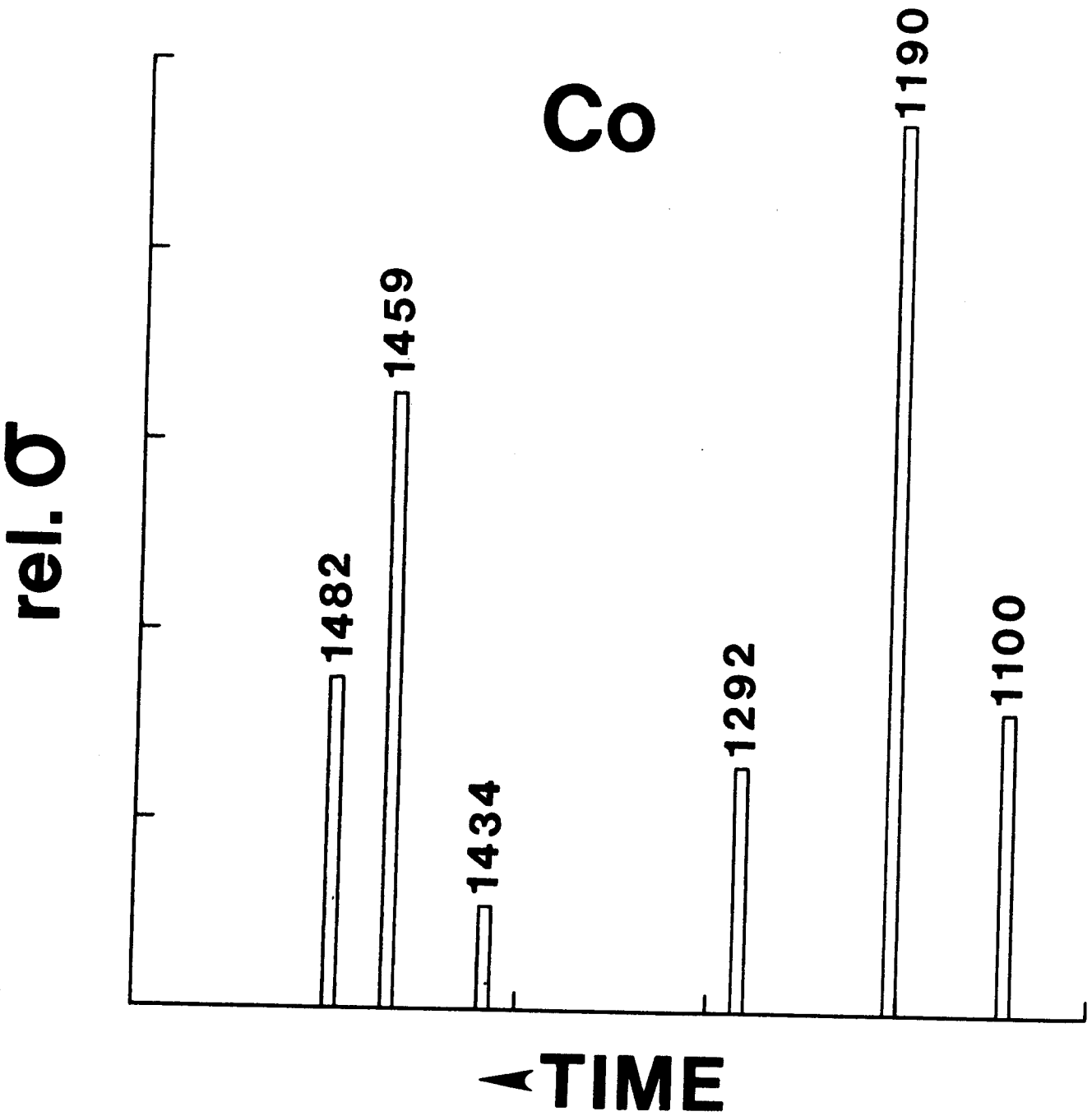

Fig. 13. Relative calculated cross sections for the excitation of the first six levels in ^{59}Co. Excitation energies are numerically given in keV. The horizontal axis has been scaled to correspond to the time spectrum of Fig. 6, and the calculated cross-section magnitudes have been corrected for detector efficiencies so as to make possible a direct comparison with Fig. 6. The incident energy is 3.0 MeV and the laboratory scattering angle 120^{o}.

V. DISCUSSION

There are a number of physical features of the above interpretation that are unusual and that will impact on the use of the OM in fundamental and applied studies. Cobalt lies near the peak of the s-wave strength function and low-energy observables, such as the $\ell = 0$ strength function and the low-energy neutron total cross sections, are very sensitive to the model parameters. These low-energy properties and the associated sensitivities are accessible only to neutron studies. The present OM is exceptional in its ability to account for both low- and high-energy phenomena in a physically satisfying manner, namely by the use of energy-dependent OM-potential geometries.

The model geometries (Eqs. (4) and (5)) resulting from the foregoing interpretation are not conventional. The real radius decreases quite sharply with increasing energy in the low-MeV region. Its magnitude at low energies is relatively large, similar to that often associated with potentials based upon low-energy phenomena such as the strength function.[5] At higher energies the real radius approaches that commonly encountered in "global" models[15], and the energy dependence becomes small. The transition between a large and small energy dependence occurs at $\approx$ 7.0 MeV. The real-potential diffuseness, a_v, is constant with energy and has a value similar to that reported in "global" models. In this mass region it is frequently found that the imaginary radius is smaller than the real radius.[1,2,57] Below 10.0 MeV the present analysis of the cobalt scattering data is consistent with this observation as r_w is $\approx$ 4% smaller than r_v over the entire energy range of the present scattering measurements. At very low energies, the absorptive potential approaches the δ-function form; i.e., $a_w \rightarrow 0$. This diffuseness rises rapidly with increasing energy, and at $\approx$ 7.0 MeV reaches a value similar to that reported from "global" analyses. Above $\approx$ 7.0 MeV, a_w can be taken to be independent of energy. Similar small values of a_w near E = 0 have also been noted near A = 90 and A = 208.[17,18] Generally, it was found that the OM potential geometries for cobalt are only weakly dependent on energy above $\approx$ 7.0 MeV (i.e., $\approx$ 19.0 MeV above the Fermi energy, E_f), while for lower energies the energy variation of r_v, r_w and a_w is quite rapid. A similar result was found in bismuth[17], where the

transition between rapid and weak energy variation occurred in the 8.0 - 10.0 MeV region (i.e., $\approx$ 16.0 MeV above E_f). The difference between the transition energies in the two nuclei, referred to E_f, may be within the uncertainties of the respective experimental interpretations.

Now consider the strength of the imaginary OM potential. For the N = 50 closed-neutron-shell nucleus ^{89}Y and the N = 126 nuclide ^{209}Bi, the volume-integral-per-nucleon of the imaginary potential, J_w, has the value 66.47 and 33.87 MeV-fm^3, respectively, for E = 0.[17,18] This is to be contrasted with the large value, J_w = 135 MeV-fm^3, given in Eq. (7) for ^{59}Co. Thus, as has been noted before[58], the value of J_w increases markedly as one moves away from closed shells. This is not surprising as the imaginary potential reflects the effects of open channels not explicitly taken into account in the OM calculations. Since the further one is away from a closed shell the more channels one neglects and hence the larger the value of J_w. An additional factor contributing to the large J_w value for ^{59}Co is probably due to collective effects, as discussed below. The energy dependence of J_w, given in Eq. (7), is surprising. As the incident-neutron bombarding energy increases, more channels open up and one would expect J_w to increase with increasing E at relatively low energies.[59,60] Just the opposite energy trend results from the present interpretation, and has been reported elsewhere for this mass region; for example, by Wilmore and Hodgson.[61] This energy dependence of J_w may be attributed to the possible vibrational character of nuclei in this mass region as follows.

It is well known that the nickel isotopes can be described by the spherical shell model[62] provided that one introduces a rather large effective neutron charge to explain the observed B(E2) values. Alternatively, one can interpret the spectra of these nuclei using the vibrational model.[63] Consequently, the properties of the spherical OM were examined to assess the

effects of its use in describing neutron scattering from a vibrational nucleus. For this purpose, pseudo data for neutron shape-elastic scattering were generated for ^{60}Ni using a vibrational model in which the 0^+ ground state, the 2^+ one-phonon level at 1.333 MeV, and the two-phonon triplet, consisting of the 2^+ 2.159 MeV, the 0^+ 2.285 MeV and 4^+ 2.506 MeV levels, were coupled.[56] A potential consisting of Woods-Saxon real, derivative Woods-Saxon imaginary and Thomas spin-orbit terms was assumed. Pseudo data were then generated using the coupled-channels computer code ANLECIS[55], with the potential parameters

$$\begin{aligned} &V(\text{real}) = (47.0 - 0.3\cdot E) \quad \text{MeV} \\ &r_v = 1.28 \quad \text{fm} \\ &a_v = 0.64 \quad \text{fm} \\ \\ &W(\text{imaginary}) = (9.7 + 0.2\cdot E) \quad \text{MeV} \\ &r_w = 1.25 \quad \text{fm} \\ &a_w = 0.40 \quad \text{fm} \\ \\ &V_{so}(\text{spin-orbit}) = 6.0 \quad \text{MeV} \\ &r_{so} = 1.28 \quad \text{fm} \\ &a_{so} = 0.64 \quad \text{fm} \end{aligned} \tag{9}$$

and

$$\beta_2 = 0.25.$$

These shape-elastic-scattering pseudo data were calculated at twelve incident energies between 4.5 and 10.0 MeV, corresponding to the values of the present ^{59}Co measurements. The resulting cross sections, evaluated at 3^o steps, were truncated to the experimentally accessible 18^o to 156^o angular range. A constant error of 3% was assigned to these pseudo data, and the calculated total cross sections added, with a weight of six differential cross-section values, to form a pseudo-experimental data base for fitting with the spherical optical-model code ABAREX[45] in a manner anologous to that employed in the above interpretation. In this fitting the spin-orbit potential was held fixed. The following results were obtained.[64] Although the diffusenesses had a slight energy dependence, $a_v = (0.668 - 0.009\cdot E(\text{MeV}))$ fm and $a_w = (0.427 + 0.005\cdot E(\text{MeV}))$ fm, their values were quite similar to those of Eq. (9), which

were used to generate the pseudo data. Furthermore, the resulting real-potential radius, $r_v = 1.264$ fm, was only 1.25% smaller than that originally assumed (Eq. (9)), and the real potential strength, J_v, was only 3.7% smaller at 4.5 MeV and 4.6% smaller at 10.0 MeV. On the other hand, the imaginary-potential radius, $r_w = 1.171$ fm, resulting from the fitting was significantly smaller, 6.3%, than the original value of Eq. (9). Moreover, the character of the imaginary strength, J_w, was changed completely. From Eq. (9) it follows that the strength <u>increases</u> with increasing energy as

$$J_w = (79.94 + 1.65 \cdot E) \quad \text{MeV-fm}^3, \qquad (10\text{-a})$$

whereas a best fit to the pseudo data gives a J_w that <u>decreases</u> with energy as

$$J_w = (121.08 - 1.41 \cdot E) \quad \text{MeV-fm}^3. \qquad (10\text{-b})$$

Moreover, the zero-energy magnitude of J_w following from the fit is $\approx$ 50% larger than the original value. Somewhat similar results have been reported by Perey in his studies of charged-particle scattering.[65]

Thus, as might have been expected, when a spherical model is used to interpret pseudo data from a vibrational nucleus in this mass region there are major changes in the imaginary potential. In particular:

(i) The imaginary-potential radius is significantly smaller than that used to generate the pseudo data. This is consistent with the above experimental interpretation where r_w is $\approx$ 4% smaller than r_v, Eq. (5).

(ii) The imaginary-potential strength at E = 0 obtained from fitting the pseudo data is $\approx$ 50% stronger than that used to generate the pseudo data. Futhermore, the strength decreases with increasing energy (compare Eqs. (10-a) and (10-b)). The latter result may provide an explanation of the unphysical energy-dependence of J_w, Eq. (7), obtained by fitting the experimental ^{59}Co data where neutron-scattering data for a

vibrational nucleus was fitted using a spherical OM. The large J_w magnitudes observed at zero energy in the experimental interpretation may be considerably distorted for the same reason but still remain significantly larger than those found at neutron-shell closures.

Now consider the real-potential strength, J_v. Using only the 4.5 to 10.0 MeV data, a satisfactory fit to the values needed to describe the experiment is given by

$$J_v = (505.93 - 5.98 \cdot E) \text{ MeV-fm}^3, \qquad (11)$$

which leads to an rms deviation of 4.95 MeV-fm^3 in any of the twelve fitted points. When the three low-energy results shown in Fig. 10, corresponding to averages of the experimental data over $\approx$ 1.0 MeV intervals, are included, the constants of Eq. (11) are only slightly changed, but the rms deviation increased to 6.01 MeV-fm^3. When Eq. (11) for J_v is used, in conjunction with the geometric parameters of Eq. (5), the predicted neutron total cross section in the 1.0 to 2.0 MeV region and the s-wave strength function are not in very good agreement with those derived from experiments. Moreover, the rapid decrease in J_v with energy leads to unsatisfactory values of the predicted total cross section at energies $> \approx$ 12.0 MeV. In order to remedy both of these deficiencies, the parametrization of J_v given by Eq. (7) was chosen. Thus, when data outside the 4.5 to 10.0 MeV range are included in the considerations, one is led to the conclusion that J_v exhibits a rapid decrease with increasing energy below $\approx$ 7.0 MeV. Above that energy the slope is smaller and is quite close to Rapaport's "global" value[15], $dJ_v/dE = -2.712$ fm^3, and to the Walter and Guss result[53], $dJ_v/dE = -2.776$ fm^3. A similar result-- a large negative slope at low energies changing to a smaller value at $\approx$ 10.0 MeV-- has recently been found in an analysis of neutron scattering from ^{209}Bi.[17]

In a series of recent papers, Mahaux and Sartor[11-13] have outlined a procedure for extrapolating the OM potential to the bound-state regime. There is a well known dispersion relationship linking the real and imaginary potentials,[14]

$$V(r,E) = V_{hf}(r,E) + \frac{P}{\pi}\int_{-\infty}^{+\infty}\frac{W(r,E')}{E - E'}\,dE', \qquad (12\text{-}a)$$

where P is the principal-value integral and V_{hf} is the Hartree-Fock component of the potential. This same dispersion relationship holds for the radial moments of the potential, that is

$$\langle r(E)^q\rangle_v = \langle r(E)^q\rangle_{hf} + \frac{P}{\pi}\int_{-\infty}^{+\infty}\frac{\langle r(E')^q\rangle_w}{E - E'}\,dE', \qquad (12\text{-}b)$$

where, for example,

$$\langle r(E)^q\rangle_w = \frac{4\pi}{A}\int_0^{\infty} W(r,E)\, r^q\, dr. \qquad (13)$$

Mahaux and Sartor argue that the energy dependence of the radial moments of $\langle r(E)^q\rangle_w$ can be parametrized by the form

$$\langle r(E)^q\rangle_w = \frac{C_q\cdot(E - E_f)^2}{(E - E_f)^2 + D_q^2}, \qquad (14)$$

where C_q and D_q are constants to be fitted to the various moments of the imaginary potential and E_f is the Fermi energy. In addition, one expects $V_{hf}(r,E)$ to be a smooth function of energy. Hence it is reasonable to approximate its moments with

$$\langle r(E)^q\rangle_{hf} = A_q + B_q\cdot E. \qquad (15)$$

When Eqs. (14) and (15) are used, an analytic expression can be obtained for the various moments, $\langle r(E)^q\rangle_v$, of the total real potential,

$$\langle r(E)^q\rangle_v = A_q + B_q\cdot E + \frac{C_q\cdot D_q\cdot(E - E_f)}{(E - E_f)^2 + D_q^2}. \qquad (16)$$

For a given nucleus, values of $\langle r(E)^q \rangle_w$ can be deduced from a knowledge of the shape and strength of the imaginary potential. The values of C_q and D_q, Eq. (14), are then adjusted so as to reproduce these results. Finally, A_q and B_q of Eq. (16) are determined from a best fit to $\langle r(E)^q \rangle_v$ for $E > 0$. Eq. (16) is assumed to hold true for all values of E including $E < 0$. If one takes V(r,E), Eq. (12-a), to be a Woods-Saxon potential with a strength V_o, radius r_v and diffuseness a_v, Eq. (16) with $q = 0.8$, 2 and 4 can be used to determine these three parameters for $E < 0$. In this way Mahaux and Sartor found values of V_o, r_v and a_v which satisfactorily reproduce the bound-state data for ^{89}Y and ^{208}Pb. Moreover, in the energy domain $E_f \leq E \leq 0$, r_v decreased with increasing binding energy.

The same analysis, as outlined above, was used to determine the bound-state ^{59}Co potential using the values of $\langle r(E)^q \rangle_v$ and $\langle r(E)^q \rangle_w$ found in the preceding section. Since for incident neutron energies between 0 and 10.0 MeV, J_w, given by Eq. (7), decreases in value, the simple expression, Eq. (14), cannot be used to parametrize the moments of the imaginary potential. We have therefore replaced Eq. (14) with

$$\langle r(E)^q \rangle_w = \alpha_q \cdot (E-E_f)^2 \cdot e^{-\beta_q (E-E_f)^2} + \frac{C_q \cdot (E-E_f)^2}{(E-E_f)^2 + D_q^2}, \qquad (17)$$

where α_q and β_q are adjustable parameters. This expression is symmetric about the Fermi energy, E_f, which was taken to be $E_f = -12.25$ MeV. For $q = 2$, $\langle r(E)^q \rangle_w = J_w$, and the parameters of Eq. (17) for $q = 2$ were adjusted to give a best fit to the sixteen values determined in the present experiments (the fifteen shown in Fig. 10 together with the $E = 0$ value given by Eq. (7)), plus the values of J_w determined from the Walter and Guss potential[53] evaluated at energies ranging from E = 15.0 to 37.5 MeV in steps of 2.5 MeV. For $q \neq 2$ the imaginary-potential geometry given by Eq. (5), together with the experimentally

derived strengths, W_0, were used to evaluate the moments for $E \leq 10.0$ MeV. These moments were combined with those evaluated from the Walter-Guss potential, again calculated from E = 15.0 to 37.5 MeV in 2.5 MeV steps. The parameters of Eq. (17) were then adjusted to give a best fit when q = 0.8 and 4. Curves resulting from this fit are shown in Fig. 14, where they are compared with the experimentally-derived values of $\langle r(E)^q \rangle_w$.

When Eq. (17) is used to parametrize the moments of the imaginary potential, the moments of the real potential are given by

$$\langle r(E)^q \rangle_v = A_q + B_q \cdot E + \frac{C_q D_q (E - E_f)}{(E - E_f)^2 + D_q^2} + F_q(\alpha_q, \beta_q, (E - E_f)), \qquad (18)$$

where $F_q(\alpha_q, \beta_q, (E - E_f))$ comes from the principal-value contribution of the exponential term of Eq. (17). This added term was evaluated numerically using the computer language SPEAKEASY.[66] The parameters A_q and B_q of Eq. (18) were then adjusted to give the best fit to the sixteen values, for each q, of $\langle r(E)^q \rangle_v$ determined from the present experimental results. For q = 2, $\langle r(E)^2 \rangle_v = J_v$, and the fifteen values shown in Fig. 10, together with E = 0 value given by Eq. (7), were used. For q = 0.8 and 4 the values of $\langle r(E)^q \rangle_v$ to be fitted were calculated using the real-potential geometry of Eq. (5).

Eq. (18) was assumed to hold for E < 0, and the form of the bound-state Woods-Saxon potential was determined from a knowledge of its q = 0.8, 2 and 4 moments. In Fig. 15 the behavior of a_v, r_v and J_v is shown over the energy range $-16.0 \leq E \leq 10.0$ MeV. For E > 0 a_v and r_v reproduce quite well the values to which they were fitted. For E < 0 r_v increases with binding energy, reaching a maximum in the energy range under consideration, at ≈ -10.0 MeV. This behavior is to be contrasted with that found for the doubly-closed-shell nucleus ^{208}Pb and the closed neutron-shell nuclide ^{89}Y where r_v decreases with

increasing binding energy in the range $E_f \leq E \leq 0$ MeV.[11,12,13] Of the three moments of the imaginary potential, $\langle r(E)^4 \rangle_w$ is the least well described by Eq. (17), exhibiting an rms deviation which is 5.6% of its asymptotic value (in contrast to 3.9% and 4.7% for q = 0.8 and q = 2, respectively). As was done by Mahaux and Sartor[13] in their study of ^{89}Y, the values of V_o and r_v obtained from a fit to only the q = 0.8 and q = 2 moments with a_v held fixed at 0.6355 fm (the value given in Eq. (5)) was examined. Again r_v increases with increasing binding energy, reaching a maximum of 1.584 fm at -10.0 MeV, which is to be compared with the value 1.648 fm at -10.0 MeV shown in Fig. 15. This increase in r_v with increasing binding energy almost certainly arises because J_w for ^{59}Co, at low energies, has an entirely different behavior than that obtained for either ^{89}Y or ^{208}Pb.

Also shown in Fig. 15 is the curve representing J_v. This has the same general form as found by Mahaux and Sartor for ^{89}Y and ^{208}Pb. In addition to the experimental values of J_v at positive energies (which were fitted by adjusting A_2 and B_2 in Eq. (18)), the values needed to reproduce the observed particle- and hole-state binding energies are shown in this figure. These experimental binding energies were determined from the mass tables[67] and the nuclear data sheets[68] for ^{57}Ni, and they have incorporated into them the appropriate (N - Z)/A correction, calculated using Rapaport's "global" model[15], and the change in A in going from ^{57}Ni to ^{59}Co. In deducing these J_v's, r_v and a_v were held fixed at the values predicted by Eq. (18), for the observed binding energy, and V_o was adjusted until agreement with the observed energy was obtained. The $f_{7/2}$ hole state requires a value of J_v approximately 13.5% greater than given by Eq. (18), whereas the average of the particle states need a J_v value that is about 8.1% smaller. These relatively large discrepancies are probably due to the fact that ^{59}Co is a vibrational nucleus which has been treated above using a spherical OM.

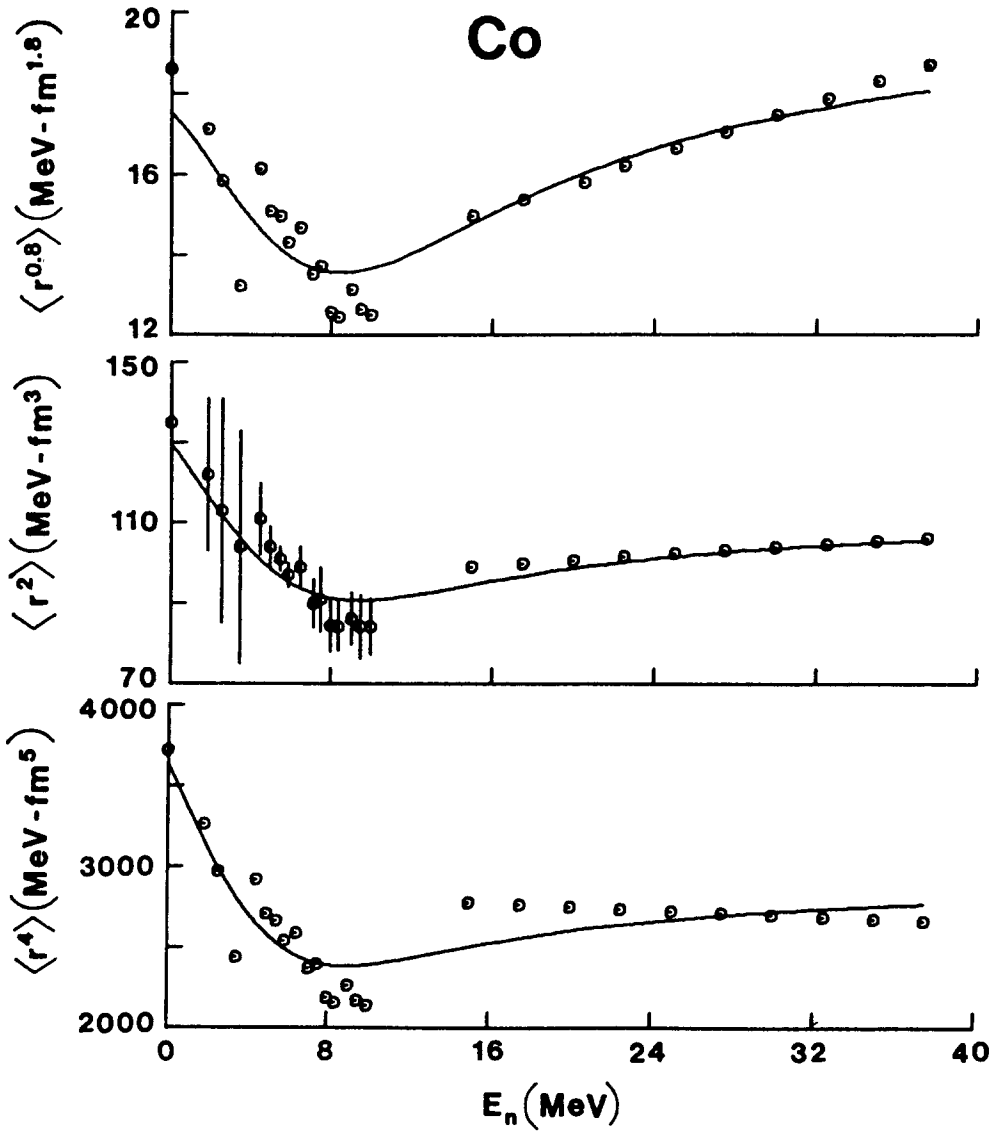

Fig. 14. Moments of the imaginary OM potential, $\langle r^q \rangle_w$, as defined by Eq. (13) of the text for q = 0.8, 2 and 4. For E ≤ 10.0 MeV the "o" symbols are values deduced from the present experiments. In the range 15.0 ≤ E ≤ 37.5 the "o" symbols represent values deduced from the Walter-Guss potential.[53] For q = 2, $\langle r(E)^2 \rangle_w \equiv J_w$ and the error estimates for E ≤ 10.0 MeV are taken from the experiments, as illustrated in Fig. 10. The solid curves are theoretical parameterizations of these moments obtained with Eq. (17) with α_q, β_q, C_q, and D_q adjusted to give a simultaneous best fit to the present data for E ≤ 10.0 MeV and to the values deduced from the Walter-Guss potential for 15.0 ≤ E ≤ 37.5 MeV, as described in the text.

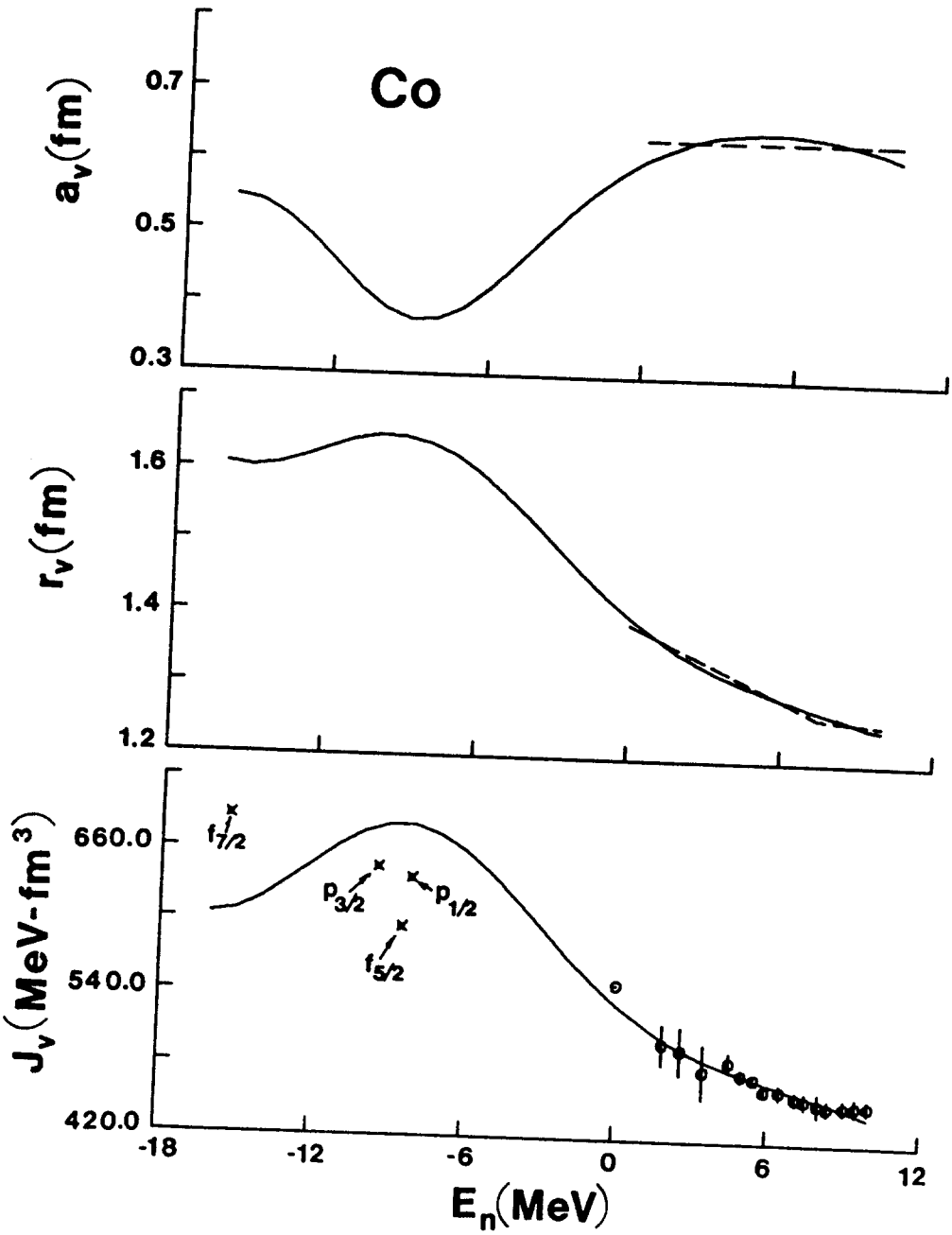

Fig. 15. Solid curves show a_v, r_v, and J_v, as a function of energy, deduced for the Woods-Saxon potential when Eq. (18) is used to determine the moments of the real well. The dashed lines correspond to the experimental values of a_v and r_v for $E \geq 0$. The J_v values and uncertainties at positive energies correspond to those shown in Fig. 10. Below zero energy the "X" symbols indicate J_v needed to give the experimental binding energies of particle- and hole-states when r_v and a_v are fixed at the values predicted by Eq. (18) for the relevant energies.

VI. SUMMARY

Energy-averaged neutron total cross sections of ^{59}Co were measured from ≈ 0.5 to 12.0 MeV together with differential elastic- and inelastic-scattering cross sections from ≈ 1.5 to 10.0 MeV. These experimental results, together with the $\ell = 0$ strength function reported from resonance measurements[48], provided the data base for spherical OM interpretations. The resulting OM potential and accompanying statistical-model calculations provided a good description of: the $\ell = 0$ strength function, the neutron total cross section (including both the low-energy region and an extrapolation to at least 20.0 MeV), differential elastic-scattering cross sections to 10.0 MeV, and of the inelastic-scattering cross sections to a few MeV. The latter calculations suggest the resolution of J^{π} ambiguities at excitation energies of ≈ 2.55 MeV. The calculations also indicate that the temperature associated with the description of continuum inelastic scattering, competing with scattering to resolved exit channels, is somewhat larger than suggested by Gilbert and Cameron.[47] For incident-neutron energies above 3.0 MeV, both the magnitude and angular distribution of observed inelastic scattering to the states between 1.0 and 1.8 MeV excitation energy suggests a substantial direct-reaction component, and for $E \geq 5.0$ MeV this is the dominant excitation mechanism for these states. A quantitative description of this direct-reaction process is provided by the weak-coupling model in which the $f_{7/2}$ proton hole in ^{59}Co is coupled to the yrast 2^+ state in ^{60}Ni. This concept accounts for five of the seven negative-parity states below 1.8 MeV. The remaining two states possess appreciable single-particle strength. Assuming that ^{60}Ni is a vibrational nucleus with $\beta_2 = 0.25$, calculations coupling the 0^+ (ground state), the 2^+ (one-phonon), and the 2^+, 0^+, 4^+ (two-phonon) states resulted in direct-excitation cross sections and angular ditributions that, when combined with the statistical contribution, describe quite well the observed excitation of levels with $E_x \leq 1.8$ MeV (see Figs. 7 and 8).

The spherical OM parameters obtained in the present interpretation are strongly energy dependent in both strength and geometry (Eqs. (5) and (7)). In particular: i) the real radius is large at low energies and rapidly decreases with increasing energy to ≈ 7.0 MeV, and then decreases much more slowly with

energy in a manner consistent with "global" models[15], ii) the real diffuseness is energy independent, iii) the energy dependence of the imaginary radius follows that of the real radius but the magnitude is ≈ 4% smaller throughout, iv) the imaginary diffuseness approaches the δ-function value, $a_w \rightarrow 0$, at zero energy, rapidly increases with energy to ≈ 7.0 MeV, and then becomes approximately constant with energy, v) the real potential strength (expressed in terms of the volume-integral-per-nucleon, J_v) decreases rapidly with increasing energy to ≈ 7.0 MeV, and then more slowly at higher energies in the manner reported for "global" models[15], and vi) the imaginary strength (expressed as the volume-integral-per-nucleon, J_w) is large and decreases with increasing energy. Characteristics i) through v) are qualitatively similar to those recently reported in the A = 90 and 208 regions[17,18], though the quantitative magnitudes are somewhat different. The break in the energy dependence of the present ^{59}Co potential occurs ≈ 19.0 MeV above the Fermi energy, whereas the similar break in the ^{209}Bi potential is at ≈ 16.0 MeV. The energy difference between the two break points may be within the experimental uncertainty as the transition is relatively slow and thus the break point not well defined. This energy dependence of both geometry and strength of the OM potentials makes possible a good description of the observables over a wide energy range, including agreement with the data at lower energies. This latter agreement is not generally achieved with potentials having energy-independent geometries. Finally, the somewhat-large value of the strength and the anomolous energy dependence of J_w (property vi) may be in part due to the use of the spherical OM to interprete neutron scattering from a vibrational nucleus. In particular, it was shown that a spherical description of the neutron scattering from a vibrational nucleus will result in a change in the imaginary potential relative to the one used in the coupled-channels calculation, in which: a) the radius is reduced by ≈ 6%, b) the strength is increased by ≈ 50%, and c) there is a change from increasing to decreasing strength as a function of incident-neutron energy. All of these characteristics are found in the present OM interpretation of ^{59}Co.

The OM derived from the neutron-scattering results was extrapolated to the bound-state regime using the dispersion relation[14] and the method of moments recently outlined by Mahaux

and Sartor.[11,12,13] The imaginary-potential moments, $\langle r^q \rangle_w$ (q = 0.8, 2 and 4), defined by Eq. (13), were parameterized by an expression symmetrical about the Fermi energy, Eqs. (17), with C_q, D_q, α_q and β_q derived by fitting the results of the present interpretation of neutron scattering from ^{59}Co, extended to ≈ 40.0 MeV using the potential of Walter and Guss.[53] The additional constants, A_q and B_q of Eq. (18), needed to parameterize the real moments were determined by fitting to the the values found in the present analysis of the 0 to 10.0 MeV ^{59}Co data. Extrapolated to bound energies, this parameterization indicates a minimum in the real diffuseness and a maximum in the real radius at ≈ -10.0 MeV. The behavior of r_v, which increase with increasing binding energy, is the opposite of that found in ^{89}Y and ^{208}Pb where r_v becomes smaller as one approaches the Fermi energy.[11,12,13] This difference undoubtedly reflects the energy dependence of the imaginary potential at low energies which, as discussed above, is quite different from that reported for ^{89}Y and ^{208}Pb. On the other hand, J_v peaks at ≈ -10.0 MeV, in the same general manner as found by Mahaux and Sartor for ^{89}Y and ^{208}Pb.[11,12,13] The average J_v implied by the ^{59}Co bound particle states is ≈ 8% smaller than that obtained from the moments analysis, and that of the hole state ≈ 13% larger. Either particle- or hole-state strengths are much larger than a linear extrapolation of the J_v values implied by the higher-energy (e.g., ≥ 7.0 MeV) neutron-scattering data, or by global models.[15,53] Clearly, there is a strong rise in J_v with decreasing energy at low positive energies, continuing into the bound-energy regime, and culminating in a maximum at ≈ -10.0 MeV.

The present (and any similar) study was inherently limited by fluctuations in the observables at low (few-MeV) energies making it very difficult to determine the energy-averaged behavior of the observables in a manner consistent with the concept of the OM. Further, there are limitations and/or distortions in a spherical OM intepretation of neutron scattering from ^{59}Co due to collective aspects of the interaction that are clearly manifest in some of the observables.

ACKNOWLEDGMENTS

The authors are pleased to acknowledge the assistance of Mr. J. Fabish and Mr. V. Svirtun in this work.

References

[1] B. Holmqvist and T. Wiedling, Aktiebolaget Atomenergi Report, AE-430 (1971) unpublished.

[2] D. Wilmore and P. E. Hodgson, Atomic Energy Research Establishment Report, AERE-R-11439 (1984) unpublished: see also J. Phys. G11 1007 (1985).

[3] P. Guenther, A. Smith and J. Whalen, Nucl. Sci. and Eng. 82, 408 (1982).

[4] A. Smith, P. Guenther, D. Smith and J. Whalen, Nucl Sci. and Eng. 72, 293 (1979).

[5] P. A. Moldauer, Nucl. Phys. 47, 65 (1963).

[6] A. Smith and P. Guenther, Proc. Conf. on Nucl. Structure Study with Neutrons, page 508, Antwerp, North-Holland Pub. Co., Amsterdam (1965).

[7] A. B. Smith, P. T. Guenther and R. D. Lawson, Nucl. Phys. A455, 344 (1986).

[8] P. A. Moldauer, Nucl. Phys. A344, 185 (1980).

[9] W. P. Poenitz, A. B. Smith and J. F. Whalen, Nucl. Sci. and Eng. 78, 333 (1981).

[10] H. E. Jackson, private communication (1980).

[11] C. Mahaux and R. Sartor, Phys. Rev. Lett. 57, 3015 (1986).

[12] C. Mahaux and R. Sartor, Nucl. Phys. A468, 193 (1987).

[13] C. Mahaux and R. Sartor, submitted for publication in Phys. Rev. C.

[14] See, for example, G. R. Satchler, Direct Nuclear Reactions Clarendon, Oxford (1983).

[15] J. Rapaport, Phys. Reports 87, 25 (1982).

[16] C. Mahaux and H. Ngô, Nucl. Phys. A378, 205 (1982); also Phys. Lett. 100B, 285 (1981).

[17] A. B. Smith, P. T. Guenther and R. D. Lawson, Argonne National Laboratory Report, ANL/NDM-100 (1987) unpublished; also submitted to Phys. Rev. C.

[18] R. D. Lawson, P. T. Guenther and A. B. Smith, Phys. Rev. C34, 1599 (1986).

[19] A. B. Smith, P. T. Guenther and J. F. Whalen, Nucl. Phys. A415, 1 (1984).

[20] See for example, C. Johnson, A. Galonsky and R. Kernell, Phys. Rev. C20, 2052 (1979).

[21] W. Poenitz and J. Whalen, Argonne National Laboratory Report, ANL/NDM-80 (1983) unpublished.

[22] C. Budtz-Jørgensen, P. Guenther, A. Smith, J. Whalen, W. McMurray M. Renan and I. Van Heerden, Z. Phys. 319, 47 (1984).

[23] A. Smith, P. Guenther, J. Whalen, I. van Heerden, and W. McMurray, J. Phys. G11, 125 (1985).

[24] P. Guenther, A. Smith and J. Whalen, Phys. Rev. C12, 1797 (1976).

[25] D. Miller, Fast Neutron Physics Vol.-II. Editors J. Marion and J. Fowler, Interscience Publishers, New York (1963).

[26] A. Smith, P. Guenther, R. Larson, C. Nelson, P. Walker and J. Whalen, Nucl. Intr. and Methods 50, 277 (1967).

[27] A. Smith, P. Guenther and R. Sjoblum, Nucl. Instr. and Methods 140, 397 (1977).

[28] A. Smith and P. Guenther, Argonne National Laboratory Report, ANL/NDM-63 (1982) unpublished.

[29] Nuclear Standards File IAEA Tech. Report 227, Editors H. Conde', A. Smith and A. Lorenz, IAEA Press, Vienna (1983).

[30] P. Guenther, The Scattering of Fast Neutrons from the Even Isotopes of Tungsten Thesis, University of Illinois (1977).

[31] A. B. Smith and J. F. Whalen, Argonne National Laboratory Report, ANL/NDM-33 (1977) unpublished.

[32] P. T. Guenther, Proc. Conf. on Nuclear Data Evaluation Methods and Procedures, Brookhaven National Laboratory Report, BNL-NCS-51363 (1980) unpublished.

[33] ENDF/B-V Carbon Evaluation, Evaluators C. Fu and F. Perey, numerical values given in Nuclear Data Standards for Nuclear Measurements, IAEA Tech. Report 227, IAEA Press, Vienna (1983).

[34] ENDF/B-V Cobalt Evaluated Data File, National Nuclear Data Center,Brookhaven National Laboratory, see for example the Brookhaven National Laboratory. Report, ENDF-328 (1982) unpublished.

[35] W. Kinney and F. Perey, Oak Ridge National Laboratory Report, ORNL-4549 (1970) unpublished.

[36] J. Brandenberger, D. Glasgow, M. McEllistrem and D. Velkley, Adena Corp. Quarterly Report #7 (1973) unpublished.

[37] P. Guenther, P. Moldauer, A. Smith and J. Whalen, Nucl. Sci. and Eng. 54, 273 (1974); also Argonne National Laboratory Report, ANL/NDM-1 (1973) unpublished.

[38] A. Smith, C. Engelbrecht and D. Reitmann, Phys. Rev. 135, 76 (1964).

[39] Nuclear Data Sheets 39, 641 (1983), P. Andersson, L. Ekstrom and J. Lyttkens (we use the values given on p-654, derived from (n;n',γ) measurements as being the more comprehensive and representative of neutron-induced processes); D. Kaipov et al., Yad. Fiz. 36, 273 (1982); D. Kaipov et al., Izv. Akad. Nauk USSR ser. Fiz. 43, 37 (1979).

[40] D. L. Broder et al., Proc. Helsinki Conf. on Nuclear Data for Reactors 2, 295 (1970).

[41] S. Mathur et al., Texas Nuclear Corp., data available at the National Nuclear Data Center, Brookhaven National Laboratory (1986).

[42] V. Scherrer, B. Allinson and W. Faust, Phys. Rev. 96, 386 (1954).

[43] L. Cranberg and J. Levin, Phys. Rev. 103, 343 (1956).

[44] See for example, P. E. Hodgson, Nuclear Reactions and Nuclear Structure Clarendon, Oxford (1971).

[45] ABAREX, A spherical optical-model code, P. A. Moldauer, private communication (1983), and as revised by R. D. Lawson (1986).

[46] W. Hauser and H. Feshbach, Phys. Rev. 87, 366 (1952).

[47] A. Gilbert and A. Cameron, Can. Jour. Phys. 43, 1446 (1965).

[48] S. F. Mughabghab, M. Divadeenam and N. E. Holden, Neutron Cross Sections, (Academic Press, New York, 1981) vol. 1, pt A.

[49] M. Sugimoto and A. B. Smith, to be published.

[50] See for example, p-91 of Ref. 44.

[51] CINDA, The index to the literature and computer files on microscopic neutron data IAEA, Vienna, (1986).

[52] National Nuclear Data Center, Brookhaven National Laboratory.

[53] R. L. Walter and P. P. Guss, in Nucl. Data for Basic and Applied Science, Edited by P. Young, R. Brown, G. Auchampaugh, P. Lisowski and L. Stewart (Gordon and Breach, New York, 1986), vol 2, p. 1079.

[54] P. Andersson, L. P. Ekstrom and J. Lyttkens, Nucl. Data Sheets 39, 641 (1983).

[55] P. A. Moldauer, ANLECIS computer code, private communication (1983).

[56] P. Andersson, L. P. Ekstrom and J. Lyttkens, Nucl. Data Sheets 48, 251 (1986).

[57] P. T. Guenther, D. L. Smith, A. B. Smith and J. F. Whalen, Ann. Nucl. Energy 13, 601 (1986).

[58] A. M. Lane, J. Lynn, E. Melkonian and E. Rae, Phys. Rev. Lett. 2, 424 (1959); W. Vonach, A. B. Smith and P. A. Moldauer, Phys. Lett. 1, 331 (1964); A. B. Smith, P. T. Guenther and J. F. Whalen, Nucl. Phys. A415, 1 (1984).

[59] R. W. Hasse and P. Schuck, Nucl. Phys. A438, 157 (1985).

[60] J. R. Rook, private communication (1986).

[61] D. Wilmore and P. E. Hodgson, Nucl. Phys. 55 673 (1964).

[62] S. Cohen, R. D. Lawson, M. H. Macfarlane, S. P. Pandya and M. Soga, Phys. Rev. 160, 903 (1967).

[63] A. K. Kerman and C. M. Shakin, Phys. Lett. 1, 151 (1962).

[64] R. D. Lawson, A. B. Smith and M. Sugimoto, Bull. Am. Phys. Soc. 32, 32 (1987).

[65] F. G. Perey, Phys. Rev. 131, 745 (1963).

[66] S. Cohen and S. C. Pieper, The Speakeasy-3 Reference Manual, Argonne National Laboratory Report, ANL-8000, Revision 1, (1976) unpublished.

[67] A. H. Wapstra and K. Bos, Atomic Data and Nuclear Data Tables 19, 177 (1977).

[68] T. W. Burrows and M. R. Bhat, Nuclear Data Sheets 47, 1 (1986).